NASA TECHNICAL NOTE

ANALYTIC STUDIES OF SOUND PRESSURES INSIDE THE DUCT OF DUCTED PROPELLERS

by Joseph A. Drischler

Langley Research Center
Hampton, Va. 23365

NATIONAL AERONAUTICS AND SPACE ADMINISTRATION • WASHINGTON, D. C. • SEPTEMBER 1971

1. Report No.	2. Government Accession No.	3. Recipient's Catalog No.
NASA TN D-6345		

4. Title and Subtitle

ANALYTIC STUDIES OF SOUND PRESSURES INSIDE THE DUCT OF DUCTED PROPELLERS

5. Report Date: September 1971

6. Performing Organization Code:

7. Author(s)

Joseph A. Drischler

8. Performing Organization Report No.: L-7378

9. Performing Organization Name and Address

NASA Langley Research Center
Hampton, Va. 23365

10. Work Unit No.: 136-80-01-04

11. Contract or Grant No.:

12. Sponsoring Agency Name and Address

National Aeronautics and Space Administration
Washington, D.C. 20546

13. Type of Report and Period Covered: Technical Note

14. Sponsoring Agency Code:

15. Supplementary Notes

16. Abstract

The sound-pressure field of a rotating ducted propeller in forward flight is analyzed by replacing the duct by an infinite coaxial circular cylinder and assuming that the blade-loading distribution associated with the thrust and the torque can be represented by a distribution of acoustic pressure doublets acting at the propeller disk. Trend studies are made to ascertain the effect on the pressure distribution inside the duct of variations in propeller loading, tip clearance, free-stream Mach number, tip Mach number, and hub-tip ratio. The effect on the pressure distribution of concentrating the loading at various radial positions on the propeller blade is also investigated.

17. Key Words (Suggested by Author(s))	18. Distribution Statement
Ducted propellers Sound pressure Noise	Unclassified – Unlimited

19. Security Classif. (of this report)	20. Security Classif. (of this page)	21. No. of Pages	22. Price*
Unclassified	Unclassified	39	$3.00

*For sale by the National Technical Information Service, Springfield, Virginia 22151

ANALYTIC STUDIES OF SOUND PRESSURES INSIDE THE DUCT OF DUCTED PROPELLERS

By Joseph A. Drischler
Langley Research Center

SUMMARY

The sound-pressure field of a rotating ducted propeller in forward flight is analyzed by replacing the duct by an infinite coaxial circular cylinder and assuming that the blade-loading distribution associated with thrust and torque can be represented by a distribution of acoustic pressure doublets acting at the propeller disk. Trend studies are made to ascertain the effect on the pressure distribution inside the duct of variations in propeller loading, tip clearance, free-stream Mach number, tip Mach number, and hub-tip ratio. The effect on the pressure distribution of concentrating the loading at various radial positions on the propeller blade is also investigated.

One of the significant findings of the investigation is that the loading distribution (with the same total thrust and torque), the blade-tip clearance, and the free-stream Mach number produce considerable variations in the radial sound-pressure distribution in the field near the propeller disk but produce insignificant variations at distances greater than about one duct radius from the propeller disk. Increasing the blade-tip clearance by only a few percent of the propeller diameter decreases the overall sound-pressure level by about 6 dB in the vicinity of the propeller tip. Increasing the free-stream Mach number generally increases the sound-pressure levels inside the duct, with the greatest increases occurring near the propeller disk and along the duct wall. At a Mach number of $M = 0.7$ the sound-pressure levels along the duct wall are from 3 dB to 6 dB higher than for $M = 0$.

INTRODUCTION

At present, various types of aircraft being developed utilize ducted fans or propellers. The presence of a duct increases the propulsion performance at low speeds and permits a reduction of propeller diameter. The presence of the duct presents a structural problem not only for fans and propellers but also for compressors, and a knowledge of the sound field inside the duct is required to develop criteria for light-weight structures of sufficient acoustic-fatigue life, particularly in the critical region near the propeller disk.

In reference 1 the sound pressures inside the duct of a ducted propeller were calculated. The duct consisted of two infinite concentric circular cylinders, the inner cylinder representing the center body, and the wave equation was solved by the method of separation of variables. The thrust and the drag (torque) forces on the propeller were combined to give a resultant force in the axial direction; no free-stream velocity through the duct was considered. In reference 2 the wave equation was also solved by the same technique. A free-stream velocity was introduced and the loading on the propeller was left arbitrary. In reference 3 Tyler and Sofrin also solved the wave equation by separation of variables and used assumed duct-velocity distributions to calculate the far-field sound pressures. However, the solutions were not combined to represent loadings on the ducted propeller nor was the pressure distribution in the duct derived. Neither reference 2 nor reference 3 presents any numerical results on ducted propellers. The purpose of the present paper is to present a solution of the wave equation based on Fourier transform techniques and to present numerical results for the effects on the pressure distribution in the duct of variations in propeller loading, tip clearance, free-stream Mach number, tip Mach number, and hub-tip ratio. The effect on pressure distribution of concentrating the loading at various radial positions on the propeller blade was also investigated.

SYMBOLS

a	hub radius
A	source strength
$A_{nm}(\beta), B_{nm}(\beta)$	undetermined functions needed to satisfy boundary conditions
b	outer duct radius
B	number of blades
c	speed of sound
$H_{nm}(r)$	quantity defined by equation (A23)
I_{nm}	quantity defined by equation (A12)
J_n, Y_n	Bessel functions of first kind and second kind, respectively
k	nondimensional frequency parameter, $\frac{n\Omega b}{c} = \frac{\omega b}{c}$

M	free-stream Mach number, V/c
M_e	effective tip Mach number
M_t	rotational tip Mach number
$n = n'B$	
n'	harmonic number
n',n,m,p,q	summation indices
$(p_T)_{n'}, (p_Q)_{n'}$	pressure in n'th harmonic due to thrust and to torque, respectively
Q	total torque
$Q(\rho)/\rho$	torque per unit nondimensional length
Q_{nm}	quantity defined by equation (A9)
r_0,θ,z_0	cylindrical coordinates
r,θ,z	cylindrical coordinates normalized to outer duct radius b
r_{cp}	nondimensional center of pressure
R_e	effective distance on span of propeller blade
SPL	sound-pressure level, decibels
SPL_{ov}	overall sound-pressure level, decibels
t	time
T	total thrust
V	free-stream velocity
α_n	quantity defined by equation (A23)

β	variable of integration
$\beta_{\pm}$	notation defined by equation (A15)
γ	included angle of propeller blade considered in reference 1
δ	nondimensional propeller tip radius
$\delta(z)$	Dirac delta function
ϵ	imaginary part of k
$\zeta_n(\mu_{nm}r)$	see equation (A6)
μ_{nm}	mth root of $\zeta_n'(\mu_{nm}\sigma) = 0$
ρ_0, θ', ζ_0	coordinates of source point
ρ, θ', ζ	nondimensional coordinates of source point
$\rho\ T(\rho)$	thrust distribution, per unit nondimensional length
σ	hub-tip ratio, a/b
ϕ_0, ϕ	velocity potential
$\chi(\rho)$	function in equation (1) denoting loading distribution $\frac{B\rho\ T(\rho)}{T}$ or $\frac{B\ Q(\rho)}{\rho Q}$
ω	frequency of n'th harmonic
Ω	propeller angular velocity

ANALYSIS

The sound-pressure field of a rotating ducted propeller is analyzed on the assumption that the pressure distribution over the propeller, associated with the thrust and the torque, can be represented by a distribution of rotating acoustic pressure doublets acting

at the propeller disk and subject to uniform rectilinear motion. This work is a generalization of the work done by Garrick and Watkins, for a free propeller reported in reference 4. It is further assumed that the pressure field near the propeller can be adequately predicted by analyzing the field between two infinite coaxial circular cylinders, the inner cylinder representing the center body, usually small in ducted propellers and large in prop-fans or compressors. The analysis does not take into account reflections, such as would occur at inlets; however, these reflections are generally small for ducted fans, except possibly very near the inlet, because of the cutoff phenomena for subsonic spinning modes.

Figure 1 is a schematic of the ducted-propeller disk and the coordinate system associated with the mathematical model used in the present analysis. The entire analysis is presented in the appendix where is derived the velocity potential or Green's function which satisfies the wave equation for a pulsating source rotating with angular velocity Ω and moving in the negative z-direction with velocity V. By properly representing the forces due to thrust and torque (or drag) these sources are superimposed to yield the pressure distribution inside the duct due to B blades rotating with angular velocity Ω.

RESULTS AND DISCUSSION

Four distributions of thrust and torque are utilized to determine their effect on the pressure distribution inside the duct. The distributions are chosen so as to have the center of pressure between the 0.6- and 0.8-spanwise stations and to be representative of the loadings of most ducted propellers. All distributions are normalized so as to yield the same total thrust T and total torque Q; that is,

$$T = B\int_{\sigma}^{\delta} \rho\, T(\rho)\, d\rho$$

and

$$Q = B\int_{\sigma}^{\delta} \frac{Q(\rho)}{\rho}\, d\rho$$

where δ and σ are the nondimensional tip and hub radius, respectively.

By letting $\chi(\rho)$ denote either $\frac{B\rho\, T(\rho)}{T}$ or $\frac{B\, Q(\rho)}{\rho Q}$ the four cases considered are

$$
\left.
\begin{aligned}
&\text{Case I} \qquad \chi(\rho) = \delta(\rho - 0.8) \\
&\text{Case II} \qquad \chi(\rho) = \frac{3\rho^2}{\delta^3 - \sigma^3} \\
&\text{Case III} \qquad \chi(\rho) = \frac{J_8(\lambda_1\rho)}{\int_\sigma^1 J_8(\lambda_1\rho)\, d\rho} \qquad \left(J_8(\lambda_1) = 0\right) \\
&\text{Case IV} \qquad \chi(\rho) = \frac{2\rho}{\delta^2 - \sigma^2}
\end{aligned}
\right\} \tag{1}
$$

and

$$\int_\sigma^\delta \chi(\rho)\, d\rho = 1$$

In all cases δ is chosen to equal 1.0 except for some studies of tip clearance in Case IV which are discussed subsequently. Case I assumes that all the thrust and all the torque are concentrated at an effective radius equal to 0.8 of the duct radius. This same assumption is discussed in reference 4 for a free propeller. Case II represents a parabolic loading distribution and Case III is loaded according to $J_8(\lambda_1\rho)$ which has its center of pressure at approximately 0.75 the blade radius with $J_8(\lambda_1) = 0$ where λ_1 is the first root of $J_8(x) = 0$. Case IV represents a linear loading distribution. For comparison, the four basic types of propeller loading are presented in figure 2 for a hub-tip ratio of 0.2. The values for the centers of pressure are also given.

Values of thrust, torque, blade radius and number, rotational speed, and blade angle for a particular ducted propeller were obtained from reference 1 and are given with other pertinent data in table I. These data are used throughout the present report for all numerical studies unless otherwise stated. Measurements and calculations were made in the U.S. Customary units. The values are presented herein in the International System of Units (SI) with the equivalent values given parenthetically in the U.S. Customary Units.

Radial Pressure Distribution

In figures 3 to 6 the overall root-mean-square (rms) radial pressure distribution is presented for $M = 0$ at various values of z, the distance from the propeller disk. The nondimensional radial coordinate varies from $r = 0.2$ at the hub to $r = 1.0$ at the

duct wall. It can be seen in figure 3 that large differences occur in overall sound-pressure level SPL_{OV} among all four cases, the greatest difference being in Case I at $r = 0.8$ where the loading is concentrated. Farther downstream (figs. 4 to 6) the effect of the loading distribution becomes less apparent and, although not presented, at a station approximately one duct radius from the propeller disk, differences in the SPL_{OV} among the four cases become indistinguishable. This is as expected since examination of equations (A24) and (A25) indicates that the pressure drops off exponentially as the distance from the propeller disk increases. At $z = 0$ the exponent of the exponential vanishes and more terms are needed to define the SPL_{OV}. A further indication of this trend may be noted in figure 7 where the SPL_{OV} along the duct wall ($r = 1.0$) is plotted against z. At $z = 1.0$, although not shown, further calculations indicate that the first term dominates and the values of SPL_{OV} in all four cases converge to within 1 dB.

Whereas figures 3 to 7 show the SPL_{OV}, figures 8 to 10, in which sound-pressure level SPL is plotted against harmonic number n', show the contribution of each harmonic to the values presented in figure 7 for SPL_{OV} along the duct wall at $r = 1.0$.

In figure 8, which represents the SPL in the propeller disk, it appears that all harmonics shown contribute significantly to the SPL_{OV}, an indication that the 20 terms used in the series and as mentioned in the appendix were insufficient to determine the pressure in the plane at $z = 0$. This is due to the fact the exponent of the exponential is zero in the propeller disk whereas, downstream of the disk (at $z = 0.06$ and at $z = 0.1$ in figs. 9 and 10, respectively), since the series converges rapidly, the contribution from the higher harmonics falls off with increasing harmonic number. It may also be noted in figures 9 and 10 that downstream of the propeller disk, in the first two harmonics, values of SPL agree to within 3 dB for all four cases; however, in the higher harmonics there are large differences which are believed to be due to the details of the different loading distributions.

Effect of Tip Clearance

In reference 1 are presented the results of some experimental measurements of the effect of tip clearance on the overall sound-pressure level in the duct. These measurements are taken on the propeller for which the parameters are given in table I except that values of thrust and torque are replaced by $T = 5224.6$ N (1174.6 lbf) and $Q = 1783$ J (1315 ft-lbf) to correspond with the experimental results presented in figure 17 of reference 1.

In the present paper only Case IV (linear loading) is considered to illustrate the effect of tip clearance. The clearances used herein are the same as those of reference 1, namely, 0.95 cm (3/8 in.) and 3.81 cm (1.5 in.), which correspond to values of nondimensional blade tip radius equal to 0.991 and 0.964, respectively. The effect on the SPL_{OV}

across the propeller disk is shown in figure 11 and along the duct wall ($r = 1.0$), in figure 12. Here it can be seen (fig. 11) that the tip clearance is effective in reducing the SPL_{OV} over only the outer 5 percent of the disk and has a negligible effect on the remaining portion of the disk. However, as mentioned previously, and in the appendix, the results for $z = 0$ (at the propeller disk) are questionable. Along the duct wall (fig. 12) the effect seems to extend from $z = 0$ to approximately $z = 0.2$. This reduction in pressure could be significant in the structural design of ducted propellers; however, the loss of performance may be more important in determining the design criteria.

Also plotted in figure 12 are the experimental data obtained from figure 17 of reference 1. The symbols with ticks represent data points taken upstream of the propeller disk and are included in figure 12 since the present analysis indicates equal attenuation in both directions. As can be seen in figure 12, the measured pressures upstream of the disk are greater than those downstream and the differences due to tip clearance are much greater than those indicated by the theory. The overall agreement between experimental and theoretical results is felt to be poor and no explanation of these differences can be given at the present time.

Effects of Free-Stream Mach Number

Two different free-stream Mach numbers were considered for comparison with the static case $M = 0$, namely, $M = 0.3$ and $M = 0.7$, which yield effective Mach numbers of $M_e = 0.73$ and $M_e = 0.97$, respectively. Only Case II (parabolic loading) was considered and the overall sound-pressure level is presented for $M = 0$ and $M = 0.7$ in figures 13 and 14. The results for $M = 0.3$ are not shown since they are essentially the same as those for $M = 0$. In figure 13, the SPL_{OV} at the duct wall shows an increase of between 3 dB and 6 dB due to Mach number effects as the station moves downstream (or upstream) from the propeller disk at $z = 0$ to $z = 0.4$. In figure 14 it can be seen that the difference decreases as the station aproaches the hub; for $z = 0.1$ the effect of Mach number is negligible. It may be noted here, and is discussed more fully in the appendix that, for effective Mach numbers $M_e = \sqrt{M^2 + M_t^2} < 1.0$, M_t being the rotational tip Mach number, the pressure attenuates equally in both upstream and downstream directions.

Effect of Rotational Tip Mach Number

For the case of linear spanwise loading (Case IV), the effect of rotational tip Mach number is investigated for two free-stream conditions, $M = 0$ and $M = 0.7$. These results are presented in figures 15 and 16, which show the overall sound-pressure level along the duct wall for several rotational tip Mach numbers between 0.6 to 2.0. Here it can be seen that for an effective Mach number $M_e = \sqrt{M^2 + M_t^2} < 1.0$ the pressure

decreases exponentially, an indication of attenuation of the pressure waves, whereas for $M_e > 1.0$ the waves propagate in both directions with nearly equal amplitude all along the duct wall. The criterion for propagation, as mentioned previously, is discussed in the appendix; however, it may be illustrated by examining the exponential in equations (A24) and (A25). When α_n is a real quantity; that is, when

$$k^2 > \left(1 - M^2\right)\mu_{nm}{}^2$$

or

$$\left(nM_t\right)^2 > \left(1 - M^2\right)\mu_{nm}{}^2$$

the contribution from that term in the series causes propagation; otherwise the wave decays exponentially. For example, for $M = 0$ and $M_t = 1.2$, μ_{nm} must be less than $1.2n$, where $n = n'B$, in order for a wave to propagate in the duct. The tables of reference 5 show this inequality to be satisfied when $n \geqq 9$ ($n' \geqq 3$). This is further illustrated in figure 17 which gives the harmonic content of duct-wall pressure for $M = 0$ and $M_t = 1.2$. It may be noted that the pressure harmonics attenuate for $n' = 1$ and $n' = 2$ whereas the higher harmonics propagate.

Results are shown in figures 15 to 17 to indicate how various harmonics can decay or propagate depending on the effective Mach number. Although effective Mach numbers greater than one are physically possible for configurations such as prop-fans, the Mach numbers presented herein are higher than the operating range of the particular configuration considered in reference 1. Also, since figure 17 indicates that the propagating waves produce sound-pressure levels of nearly the same magnitude (at least to the tenth harmonic), it would appear inappropriate to sum algebraically the squares of the pressures in each mode. A further investigation should be undertaken to determine the manner in which the individual modes should be combined.

Effect of Hub-Tip Ratio

The effect on the overall sound-pressure level of changing the hub-tip ratio from $\sigma = 0.2$ to $\sigma = 0.5$ is illustrated in figures 18 to 20 for the linearly loaded blade (Case IV). In figure 18 the radial variation in SPL_{OV} is presented for stations $z = 0.2$ and $z = 0.4$. Here it can be seen that concentrating the loading over the outer half of the blade results in an increase in SPL_{OV} along the duct wall of approximately 2 dB to 3 dB over that for the more lightly loaded blade even though the rotation speed, thrust, and torque are the same for both cases. This same trend is also evident in figure 19, where the SPL_{OV} is given along the duct wall and the difference in decibels remains essentially constant as the station moves downstream. Also, in figure 20 where

the harmonic content of the overall SPL at $z = 0.1$ and $r = 1.0$ is shown, a difference of approximately 2 dB exists for all 10 harmonics.

Effect of Varying Effective Radius of Concentrated Load

The concept of concentrating the thrust and the torque at some effective distance R_e on the span of the blade was used by Garrick and Watkins in reference 4. The suggested value of $R_e = 0.8$ (ref. 4) is used herein, together with values of $R_e = 0.6$ and $R_e = 0.7$. The results of these calculations are presented in figures 21 to 23; figure 21 shows the variation in overall sound-pressure level in the radial direction and figure 22, the variation along the duct wall. Figure 23 shows the harmonic content of the overall sound pressure along the duct wall at $z = 0.1$ and $r = 1.0$. It can be seen from figures 21 to 23 that the effective-radius concept leads to large differences in sound-pressure level near the propeller disk. By comparing figures 7 and 21 it can be seen that, even though the concentrated-loading theory yields pressure distributions which are essentially independent of the loading as the station moves downstream in the duct, it should be used with caution near the propeller disk.

Comparison of Present Results With Reference 1

In reference 1, the wave equation for a propeller in an infinite coaxial circular cylinder is solved by separation of variables. The pressure on the propeller blade is assumed to be the resultant of two forces, the thrust acting in the axial direction and the drag acting in the circumferential direction at the center of pressure r_{cp}. The resultant of these two vectors, that is,

$$P_0 = \sqrt{T^2 + \left(\frac{Q}{r_{cp}}\right)^2}$$

was assumed to be distributed uniformly over the blade (a sector of angle γ) and to act in the axial direction. The absolute value of the Fourier coefficient of the n'th harmonic for the loading can be represented by

$$\left|\left(P_0\right)_{n'}\right| = \frac{P_0}{\pi b^2\left(1 - \sigma^2\right)} \left|\frac{\sin \frac{n'\gamma B}{2}}{\frac{n'B\gamma}{2}}\right| \tag{2}$$

This loading differs from the loading considered in the present paper where the thrust and the torque are considered concentrated along radial lines and thus yielding a comparable equation

$$\left|\left(P_0\right)_{n'}\right| = \frac{P_0'}{\pi b^2\left(1 - \sigma^2\right)} \tag{3}$$

where P_0' is representative of either the thrust force T or the drag force Q/r_{cp}. Equations (2) and (3) have the same form as $\gamma \to 0$.

Circumferential integration over each blade considered in reference 1 results in a linear pressure variation in the radial direction and thus is comparable to case IV $\left[\chi(\rho) = \frac{2\rho}{1 - \sigma^2}\right]$ considered herein. By using the notation of the present paper, the n'th harmonic of the pressure distribution presented in reference 1 can be written in the form

$$\left(p_{rms}\right)_{n'} = \left|\frac{8\sqrt{2}\,P_0 \sin\frac{n\gamma}{2}}{n\gamma b^2\left(1 - \sigma^2\right)}\right| \left[\sum_{m=1} \left| H_{nm}(r)\,\alpha_n \int_\sigma^1 \rho\,\zeta_n\left(\mu_{nm}\rho\right) e^{-i\alpha_n z}\,d\rho \right|^2\right]^{1/2} \tag{4}$$

and

$$p_{rms} = \left\{\sum_{n'=1} \left[\left(p_{rms}\right)_{n'}\right]^2\right\}^{1/2}$$

where, as before, $n \equiv n'B$. A comparison of equations (A24) and (4) shows that with the exception of the loading, the pressure distribution in the duct is given, in the present analysis, as the sum of the radial modes whereas, in reference 1, the pressure distribution is the square root of the sum of the squares of the radial modes.

Figure 24 shows the harmonic content of the overall SPL for some calculations based on equations (4) and (A24), together with experimental data from figure 31 of reference 1. The data were obtained from reference 1 and are for $z = 0.104$, $r = 1.0$, and $M = 0$. Other pertinent quantities are presented in table I, also obtained from reference 1. In figure 24, it can be seen that the results from both theories and the experimental results are in fair agreement at least to the sixth harmonic. The differences thereafter are believed to be due to the differences in the details of the loading. As noted in equation (2) the contribution from the n'th harmonic of the pressure loading is zero when $\frac{n'B\gamma}{2} = \pi$ or when $n' = \frac{2\pi}{B\gamma}$. Utilizing the constants $\gamma = 0.27$ rad and $B = 3$ from table I yields a value of $n' = 7.75$. Examination of figure 24 indicates a great reduction in SPL for a value of $n' = 8$ which, as mentioned previously, may be due to the differences in the details of the loading used in the present paper and that of reference 1.

SUMMARY OF RESULTS

The sound-pressure level inside the duct of a ducted propeller is analyzed by replacing the duct by an infinite coaxial circular cylinder and assuming that the blade-loading distribution associated with thrust and torque can be represented by a distribution

of acoustic pressure doublets acting at the propeller disk. Trend studies are made to determine the effect on the pressure distribution inside the duct of variations in propeller loading, tip clearance, free-stream Mach number, tip Mach number, and hub-tip ratio. The effect on pressure distribution of concentrating the loading at various radial positions on the propeller blade is also investigated.

The following results are observed:

1. The radial pressure distribution at least one radius downstream of the propeller disk is essentially independent of the blade loading; however, there is a significant variation in the field near the propeller disk.

2. Increasing the blade-tip clearance by only a few percent of the propeller diameter has a significant effect in reducing the overall sound-pressure level along the duct wall by about 6 dB in the field near the propeller disk; however, at approximately one radius from the disk, the effect of tip clearance is negligible.

3. For the angular velocity considered, free-stream Mach numbers equal to or less than 0.3 have very little effect on the pressure distribution whereas, for $M = 0.7$, the sound-pressure levels along the duct wall are from 3 dB to 6 dB higher than for $M = 0$.

4. For effective tip Mach numbers $M_e < 1$ the sound waves attenuate in the duct whereas for $M_e > 1$ the waves propagate, the sound-pressure level along the duct wall remaining essentially constant and changing only near the propeller disk.

5. For the case with linear distribution and the same total load, increasing the hub-tip ratio from $\sigma = 0.2$ to $\sigma = 0.5$ results in an increase in sound-pressure level of approximately 2 dB to 3 dB throughout the duct.

6. Changing the location of the effective radius R_e of the concentrated load results in significantly different sound-pressure levels near the propeller disk. As R_e is increased the pressures on the outer wall increase and those on the inner wall decrease; however, as pointed out previously in item (1), as the distance downstream increases, the pressure distribution across the duct becomes independent of the load distribution.

7. As the effective radius is decreased, the sound-pressure levels in the higher harmonics rapidly decrease, so that it is necessary to calculate only a few harmonics to determine the overall sound-pressure level.

Langley Research Center,
National Aeronautics and Space Administration,
Hampton, Virginia, June 23, 1971.

APPENDIX

SOUND-PRESSURE LEVEL INSIDE AN INFINITE ANNULAR DUCT

The purpose of the appendix is to derive the pressures due to thrust and torque in an annular duct containing uniform subsonic or supersonic flow. First, expressions are derived to give the pressures due to unit pulsating forces acting in the axial direction to simulate the thrust and in the tangential direction to simulate the torque, or drag. By superposition, the forces are combined in such a way as to represent the thrust and the torque distribution on a propeller in the duct. A Fourier time expansion of the thrust and the torque is made to account for the rotating blades. This procedure allows each blade harmonic to be treated as a distribution of pulsating forces.

Derivation of Pressure Due to Concentrated Pulsating Force in Duct of Infinite Length

The velocity potential due to a pulsating source of strength A in an annular duct with free-stream velocity V directed along the positive Z_0-axis is governed by the wave equation

$$\nabla^2 \phi_0 = \frac{1}{c^2}\left(V\frac{\partial}{\partial z_0} + \frac{\partial}{\partial t}\right)^2 \phi_0 + \frac{Ae^{-i\omega t}}{\rho_0}\delta\left(r_0 - \rho_0\right)\delta\left(z_0 - \zeta_0\right)\delta(\theta - \theta') \tag{A1}$$

with boundary conditions such that the velocity normal to the duct walls be zero; that is,

$$\left[\frac{\partial \phi_0}{\partial r_0}\right]_{r_0=a} = \left[\frac{\partial \phi_0}{\partial r_0}\right]_{r_0=b} = 0$$

where $r_0 = a$, the inner or hub radius, and $r_0 = b$, the outer or wall radius. In equation (A1), r_0, θ, and z_0 are the coordinates of the field point and ρ_0, θ', and ζ_0 those of the source point. Figure 1(a) is a schematic of the propeller disk and the coordinate system associated with equation (A1). Figure 1(b) is the mathematical model used in the present analysis. The coordinates are normalized with respect to the outer-duct radius where $r = \sigma$ $\left(\sigma = \frac{a}{b}\right)$ and $r = 1.0$ correspond to the hub and the outer wall, respectively, and the duct is of infinite length ($-\infty < z < \infty$).

By letting $\phi_0 = \phi e^{-i\omega t}$ and normalizing all coordinates with respect to b, equation (A1) becomes

$$\left(1 - M^2\right)\frac{\partial^2 \phi}{\partial z^2} + 2ikM\frac{\partial \phi}{\partial z} + k^2\phi + \frac{\partial^2 \phi}{\partial r^2} + \frac{1}{r}\frac{\partial \phi}{\partial r} + \frac{1}{r^2}\frac{\partial^2 \phi}{\partial \theta^2} = \frac{A}{\rho b}\delta(r - \rho)\,\delta(z - \zeta)\,\delta(\theta - \theta') \tag{A2}$$

and

$$\left[\frac{\partial \phi}{\partial r}\right]_{r=\sigma} = \left[\frac{\partial \phi}{\partial r}\right]_{r=1} = 0 \tag{A3}$$

where $M = \frac{V}{c}$ and $k = \frac{\omega b}{c}$. In the following analysis it is assumed that k is a complex quantity with a positive imaginary part. This assumption is equivalent to introducing a damping term $\frac{\partial \phi_0}{\partial t}$ into the wave equation (A1). As is seen later, in connection with equation (A12), this device moves the singularities off the path of integration and simplifies the evaluation of certain integrals. The final solution is obtained by letting the imaginary part of k approach zero. A further discussion of this can be found, for example, in reference 6.

The solution of equation (A2) is assumed to have the form

$$\phi = \sum_{n=-\infty}^{\infty} e^{in\theta} \int_{-\infty}^{\infty} \left[J_n(\mu r)\, A_n(\beta) + Y_n(\mu r)\, B_n(\beta)\right] e^{-i\beta z}\, d\beta \tag{A4}$$

where $J_n(\mu r)$ and $Y_n(\mu r)$ are Bessel functions of the first and second kind, respectively, and $A_n(\beta)$ and $B_n(\beta)$ are arbitrary functions of β which must be chosen so as to satisfy the boundary conditions of equation (A3). The functions $A_n(\beta)$ and $B_n(\beta)$ are determined by substituting the expression in the square bracket in equation (A4) into equation (A3). Thus, equation (A4) becomes

$$\phi = \sum_{n=-\infty}^{\infty} \sum_{m=1}^{\infty} e^{in\theta} \frac{\zeta_n(\mu_{nm} r)}{Y_n'(\mu_{nm})} \int_{-\infty}^{\infty} A_{nm}(\beta)\, e^{-i\beta z}\, d\beta \tag{A5}$$

in which the eigenfunctions $\zeta_n(\mu_{nm} r)$ are given by

$$\zeta_n(\mu_{nm} r) \equiv J_n(\mu_{nm} r)\, Y_n'(\mu_{nm}) - J_n'(\mu_{nm})\, Y_n(\mu_{nm} r) \tag{A6}$$

and μ_{nm} is the mth eigenvalue of the characteristic equation

$$\zeta_n'(\mu_{nm} \sigma) = 0 \tag{A7}$$

where the primes are used in equations (A5), (A6), and (A7) to indicate differentiation of the function with respect to its argument. Reference 5 contains tables listing values of μ_{nm} for $n = 0$ to $n = 25$ and $m = 1$ to $m = 10$ with values of σ ranging from 0 to 0.9 in steps of 0.1. It may also be noted that

$$E(\mu_{nm}r) = \frac{\zeta_n(\mu_{nm}r)}{Y_n'(\mu_{nm})}$$

where E is the notation used by Tyler and Sofrin in reference 3.

Substitution of equation (A5) into equation (A2) yields

$$\sum_{n=-\infty}^{\infty} \sum_{m=1}^{\infty} e^{in\theta} \frac{\zeta_n(\mu_{nm}r)}{Y_n'(\mu_{nm})} \int_{-\infty}^{\infty} A_{nm}(\beta)\, e^{-i\beta z} \left[\beta^2(1 - M^2) - 2k\beta M + \mu_{nm}^2 - k^2\right] d\beta$$

$$= -\frac{A}{\rho b}\, \delta(r - \rho)\, \delta(z - \zeta)\, \delta(\theta - \theta') \quad \text{(A8)}$$

Using the orthogonal relations

$$\left.\begin{aligned} &\int_0^{2\pi} e^{i(n-n')\theta}\, d\theta = \begin{cases} 0 & (n \neq n') \\ 2\pi & (n = n') \end{cases} \\ &\text{and} \\ &\int_\sigma^1 \zeta_n(\mu_{nm}r)\, \zeta_n(\mu_{nm'}r)\, r\, dr = 0 \qquad (m \neq m') \\ &\qquad = Q_{nm} \equiv \frac{1}{2}r^2\left(1 - \frac{n^2}{\mu_{nm}^2 r^2}\right)\zeta_n^2(\mu_{nm}r)\Big|_{r=\sigma}^{r=1} \qquad (m = m') \end{aligned}\right\} \quad \text{(A9)}$$

ogether with the inverse Fourier transform with respect to β yields the expression

$$A_{nm} = \frac{-Y_n'(\mu_{nm})\frac{A}{b}\, e^{i\beta\zeta} e^{-in\theta'}\, \zeta_n(\mu_{nm}\rho)}{4\pi^2 Q_{nm}\left[\beta^2(1 - M^2) - 2\beta kM + \mu_{nm}^2 - k^2\right]} \quad \text{(A10)}$$

ff equation (A10) is substituted into equation (A5), the result can be written in the form

$$\phi(r,\rho,\bar{\theta},\bar{z}) = -\sum_{n=-\infty}^{\infty} \sum_{m=1}^{\infty} \frac{A e^{in\bar{\theta}} \zeta_n(\mu_{nm}r)\, \zeta_n(\mu_{nm}\rho)}{4\pi^2 b Q_{nm}} I_{nm} \quad \text{(A11)}$$

where

$$I_{nm} = \int_{-\infty}^{\infty} \frac{e^{-i\beta\bar{z}}\, d\beta}{(1 - M^2)\beta^2 - 2kM\beta + \mu_{nm}^2 - k^2} \tag{A12}$$

and

$$\bar{\theta} = \theta - \theta'$$

$$\bar{z} = z - \zeta$$

Here $\phi(r,\rho,\bar{\theta},\bar{z})$ is the Green's function which represents the velocity potential at r,θ,z due to a concentrated source of strength $Ae^{-i\omega t}$ located at ρ,θ',ζ in a fluid with free-stream velocity V.

Evaluation of I_{nm}, Equation (A12)

The integral I_{nm} can be evaluated by the theory of residues. To accomplish this it is necessary to investigate the zeros of the denominator of the integrand, namely

$$\beta = \frac{M(k + i\epsilon) \pm \sqrt{k^2 - (1 - M^2)\mu_{nm}^2 + 2ik\epsilon}}{1 - M^2}$$

where ϵ is the positive imaginary part of k and, as mentioned previously, has the effect of moving the poles off the path of integration. For $M > 1.0$ it can be shown that both poles lie in the lower half of the β-plane. In the limit as $\epsilon \to 0$ the path of integration passes above both poles which are located at

$$\beta = -\frac{1}{M^2 - 1}\left[Mk \pm \sqrt{k^2 + (M^2 - 1)\mu_{nm}^2}\right] \tag{A13}$$

and the value of the integral is, for $M > 1.0$,

$$\left.\begin{aligned} (I_{nm})_{M>1.0} &= \frac{-2\pi e^{ikM\bar{z}/(M^2-1)}}{\sqrt{k^2 + (M^2 - 1)\mu_{nm}^2}} \sin \frac{\bar{z}\sqrt{k^2 + (M^2 - 1)\mu_{nm}^2}}{M^2 - 1} && (\bar{z} > 0) \\ &= 0 && (\bar{z} < 0) \end{aligned}\right\} \tag{A14}$$

For $M < 1.0$ one pole lies in the upper half of the β-plane and the other in the lower half of the β-plane. In the limit as $\epsilon \to 0$ the path of integration passes between the poles which are located at

$$\beta_{\pm} = \frac{1}{1 - M^2}\left(Mk \pm \sqrt{k^2 - \left(1 - M^2\right)\mu_{nm}^2}\right) \tag{A15}$$

where the upper sign applies when the pole is in the upper half of the plane and the lower sign when the pole is in the lower half of the plane. By adopting the notation $+\sqrt{k^2 - \left(1 - M^2\right)\mu_{nm}^2} = +i\sqrt{\left(1 - M^2\right)\mu_{nm}^2 - k^2}$ equation (A15) can be rewritten

$$\beta_{\pm} = \frac{1}{1 - M^2}\left(Mk \pm i\sqrt{\left(1 - M^2\right)\mu_{nm}^2 - k^2}\right) \tag{A16}$$

where the sign convention defined in equation (A15) applies. With use of this definition there can easily be obtained, for $M < 1.0$

$$\left.\begin{aligned} \left(I_{nm}\right)_{M<1.0} &= \frac{\pi i}{\sqrt{k^2 - \left(1 - M^2\right)\mu_{nm}^2}} e^{-i\bar{z}\beta_+} && \left(\bar{z} < 0\right) \\ &= \frac{\pi i}{\sqrt{k^2 - \left(1 - M^2\right)\mu_{nm}^2}} e^{-i\bar{z}\beta_-} && \left(\bar{z} > 0\right) \end{aligned}\right\} \tag{A17}$$

Substituting either equation (A14) for $M > 1.0$ or equation (A17) for $M < 1.0$ into equation (A11) yields the velocity potential for a concentrated source of strength $Ae^{-i\omega t}$ By the proper choice of A it is shown in reference 4 that, for a force

$$T\left(\rho_0, \theta', \zeta_0\right) \rho_0 \, d\rho_0 \, d\theta'$$

acting in the z-direction, the pressure at any field point r_0, θ, z_0 can be obtained by differentiating the velocity potential with respect to z_0 and replacing A by $T\left(\rho_0, \theta', \zeta_0\right) \rho_0 \, d\rho_0 \, d\theta'$ so that

$$p_T = T\left(\rho_0, \theta', \zeta_0\right) \rho_0 \, d\rho_0 \, d\theta' \, \frac{1}{A} \frac{\partial \phi}{\partial z_0} \tag{A18}$$

or in nondimensional quantities

$$p_T = b \, T\left(\rho, \theta', \zeta\right) \rho \, d\rho \, d\theta' \, \frac{1}{A} \frac{\partial \phi}{\partial z} \tag{A19}$$

where $T(\rho,\theta',\zeta)$ is the thrust per unit area. Similarly, if A is related to

$$\frac{Q\left(\rho_0,\theta'\zeta_0\right)}{\rho_0}\,\rho_0\,d\rho_0\,d\theta'$$

a force in the tangential direction, the pressure can be expressed as

$$p_Q = Q\left(\rho,\theta',\zeta\right)\,d\rho\,d\theta'\,\frac{1}{A\rho}\,\frac{\partial\phi}{\partial\theta'} \tag{A20}$$

and $Q\left(\rho,\theta',\zeta\right)$ is the torque per unit area. The problem now remains to express (in a Fourier series) the thrust and the torque as a distribution of concentrated forces of the form $Ae^{-i\omega t}$ so that each term of the expansion is of the form for which equation (A11) was developed.

Fourier Expansion of Thrust and Torque Distribution on Rotating Blades

Each element of the propeller blade is acted on by the surface-pressure distribution which may be resolved into a thrust force in the direction of the Z-axis and a force associated with the torque acting in the circumferential direction. A description of these forces, including a discussion of the effect of blade thickness on the sound pressure, and their Fourier expansions are given in reference 4. The present analysis to this point has been general in regard to the distribution of thrust and torque; now the analysis is specialized to the case of forces on a propeller which lies in the plane where $z = 0$ and rotates with angular velocity Ω. Further, the forces are assumed to be distributed radially along B blades $\left(\text{the angle between the blades being } \frac{2\pi}{B}\right)$ and to be concentrated circumferentially at

$$\theta' = \Omega t + \frac{2\pi p}{B} \qquad \left(p = 0,1,2,\ \ldots\ (B-1)\right)$$

This can be represented by

$$\psi = \psi_0\left(\rho_0\right)\delta\left(\zeta_0\right)\sum_{p=0}^{B-1}\delta\left(\theta' - \Omega t - \frac{2\pi p}{B}\right) \tag{A21}$$

where ψ is representative of either the thrust $T\left(\rho_0,\theta'\right)$ or the drag force $Q\left(\rho_0,\theta'\right)/\rho_0$ per unit area and $\psi_0\left(\rho_0\right)$ represents the thrust or the drag force per unit length. This series when expanded in its Fourier form becomes

$$\psi = \psi_0\left(\rho_0\right)\,\delta\left(\zeta_0\right)\frac{1}{2\pi}\sum_{p=0}^{B-1}\sum_{q=-\infty}^{\infty} e^{iq\left(\theta'-\Omega t-\frac{2\pi p}{B}\right)} \tag{A22}$$

from which it can be seen that $k = \frac{q\Omega b}{c}$ and each term in the series is of the form $Ae^{-\omega t}$ for which equation (A11) was developed. It now remains to substitute the appropriate expressions in equations (A19) and (A20) for p_T and p_Q, respectively, and to integrate over the propeller disk to obtain the total pressure due to thrust and torque.

Pressure Due to Thrust and Torque

Since supersonic flow through a ducted propeller is of only academic interest, equations that apply to subsonic flow are considered from here on; however, supersonic tip Mach numbers are not excluded. Substituting the appropriate expression for ϕ from equation (A11) and for I_{nm} from equation (A17) into equation (A19) and integrating over the propeller disk gives the pressure p_T due to the thrust distribution $T(\rho)$

$$p_T = \sum_{n=-\infty}^{\infty} \sum_{m=1}^{\infty} \sum_{p=0}^{B-1} \sum_{q=-\infty}^{\infty} \frac{ie^{in\theta}\alpha_n e^{-i\alpha_n z} H_{nm}(r)}{2\pi b^2} \int_0^{2\pi} \int_\sigma^\delta e^{-in\theta' + iq\left(\theta' - \Omega t - \frac{2\pi p}{B}\right)} \zeta_n(\rho\mu_{nm})\, T(\rho)\, \rho\, d\rho\, d\theta'$$

where

$$\alpha_n = \frac{Mk \pm \sqrt{k^2 - \left(1 - M^2\right)\mu_{nm}^2}}{1 - M^2} \qquad (z \lesseqgtr 0)$$

$$H_{nm}(r) = \frac{-i\,\zeta_n(\mu_{nm} r)}{4\pi Q_{nm}\sqrt{k^2 - \left(1 - M^2\right)\mu_{nm}^2}} \qquad \text{(A23)}$$

Q_{nm} is defined by equation (A9), and σ and δ are nondimensional distances to the hub and the tip, respectively. By using the equalities

$$\int_0^{2\pi} e^{-i(n-q)\theta'}\, d\theta' = \begin{cases} 2\pi & (q = n) \\ 0 & (q \neq n) \end{cases}$$

and

$$\sum_{p=0}^{B-1} e^{-in\frac{2\pi p}{B}} = \begin{cases} B & (n = n'B) \\ 0 & (n \neq n'B) \end{cases}$$

choosing the reference angle $\theta = 0$ (since all other values of θ have, with the exception of phasing, the same time history), dropping the time factor, and combining the $\pm n$ terms, it can be shown that the n'th harmonic of the pressure due to thrust is

$$\left(p_T\right)_{n'} = \frac{i}{b^2} \epsilon_n \sum_{m=1}^{\infty} \alpha_n e^{-i\alpha_n z} H_{nm}(r) \int_{\sigma}^{\delta} B\rho\, T(\rho)\, \zeta_n\left(\mu_{nm}\rho\right) d\rho \tag{A24}$$

Similarly, the n'th harmonic of the pressure due to torque is

$$\left(p_Q\right)_{n'} = -\frac{i}{b^3} \epsilon_n \sum_{m=1}^{\infty} n e^{-i\alpha_n z} H_{nm}(r) \int_{\sigma}^{\delta} \zeta_n\left(\mu_{nm}\rho\right) \frac{B\, Q(\rho)}{\rho} d\rho \tag{A25}$$

where $\epsilon_n = 1$ for $n' = 0$ and $\epsilon_n = 2$ for $n' \neq 0$ and the root-mean-square (rms) pressure in the n'th harmonic is

$$\left(p_{rms}\right)_{n'} = \frac{1}{\sqrt{2}} \left| \left(p_T\right)_{n'} + \left(p_Q\right)_{n'} \right| \tag{A26}$$

The overall rms pressure is given by

$$p_{rms} = \left\{ \sum_{n'=1} \left[\left(p_{rms}\right)_{n'} \right]^2 \right\}^{1/2} \tag{A27}$$

and the overall sound-pressure level in decibels is given by

$$SPL_{ov} = 128 + 20 \log_{10} p_{rms} \tag{A28}$$

if p_{rms} is in lb/ft^2.

Equations (A24) to (A28) have been programed for the four thrust and torque distributions given in equation (1). The first 10 harmonics are usually presented for the conditions considered and the summation on m contains 20 terms. For values of $z > 0.1$, 5 terms appear sufficient for convergence; however, for $z = 0$, although the series appears to converge within 12 terms, it is questionable whether 20 terms are sufficient to give accurate results.

Criteria for Attenuation or Propagation of Wave in Duct

Examination of equations (A24) and (A25) shows that, when α_n is complex, certain terms in the series indicate oscillations or propagation downstream whereas when α_n is imaginary, they indicate exponential decay as z increases. This leads to an investigation of whether $k^2 - \left(1 - M^2\right)\mu_{nm}^2$ is greater than or less than zero. By substituting nM_t for k and since $M_e^2 = M^2 + M_t^2$ the expression can be rewritten as

$$M_e^2 - 1 \gtrless \left(1 - M^2\right)\left(\frac{\mu_{nm}}{n} - 1\right)\left(\frac{\mu_{nm}}{n} + 1\right) \tag{A29}$$

where, when the upper inequality in equation (A29) is satisfied, propagation is indicated and, when the lower inequality is satisfied, decay or attenuation occurs. The quantities to be examined are $M_e \gtrless 1.0$ and $M \gtrless 1.0$ For $M_e < 1.0$, which implies that $M < 1.0$, the left-hand side of equation (A29) becomes negative and the lower inequality is satisfied since, as indicated in reference 7, $\mu_{nm} > n$ and all waves attenuate. For $M_e > 1.0$, two alternatives exist, that is, $M > 1.0$ or $M < 1.0$. For $M > 1.0$, the right-hand side of equation (A29) becomes negative, the upper inequality is satisfied, and all waves propagate. For $M < 1.0$, when the approximate asymptotic expansion of the mth zero $\mu_{nm} \approx \frac{m\pi}{1 - \sigma}$ (see ref. 7) is considered it can be seen that, for a fixed m, a value can always be assigned to n for which the upper inequality is satisfied and that all circumferential modes for which the mode number is equal to or greater than this value of n propagate in the duct. It may also be noted (ref. 7) that, for large values of n, the eigenvalues are approximately the zeros of $Y_n'\left(\mu_{nm}\right) = 0$, the first eigenvalue being

$$\mu_{n,1} \approx n + 1.82n^{1/3}$$

When this expression is substituted into equation (A29) it can be seen that $M_e^2 - 1$ is of the order of $1/n^{2/3}$, again an indication that for a large enough value of n the upper inequality is satisfied and all modes with mode numbers greater than or equal to this value of n also propagate. This is also illustrated in figure 17 and mentioned in the text, that for $M_t = M_e = 1.2$ and $M = 0$, the first two modes attenuate whereas the remaining modes propagate. It therefore can be concluded that for $M_e > 1.0$ an infinite number of modes, but not all, propagate and for $M_e < 1.0$ all modes attenuate.

REFERENCES

1. Fricke, W.; Bissell, J. R.; Bamberg, W. T.; and Martina, C. K.: Analytical and Experimental Studies of Sound Pressures on Ducted Propellers. NASA CR-66270, 1966.

2. Slutsky, Simon: Discrete Noise Generation and Propagation by a Fan Engine. Paper presented at AFOSR-UTIAS Symp. on Aerodyn. Noise (Toronto), May 20-21, 1968.

3. Tyler, J. M.; and Sofrin, T. G.: Axial Flow Compressor Noise Studies. SAE Trans., vol. 70, 1962, pp. 309-332.

4. Garrick, I. E.; and Watkins, Charles E.: A Theoretical Study of the Effect of Forward Speed on the Free-Space Sound-Pressure Field Around Propellers. NACA Rep. 1198, 1954. (Supersedes NACA TN 3018.)

5. Bauer, Helmut F.: Tables of Zeros of Cross Product Bessel Functions $J_p'(\xi)Y_p'(k\xi) - J_p'(k\xi)Y_p'(\xi) = 0$. Math. Comput., vol. 18, no. 85, Jan. 1964, pp. 128-135. MTP-AERO-63-50, NASA George C. Marshall Space Flight Center, 1963.

6. Morse, Philip M.; and Feshbach Herman: Methods of Theoretical Physics. Pt. II, McGraw-Hill Book Co., Inc., 1953, pp. 1334, 1335.

7. Abramowitz, Milton; and Stegun, Irene A., eds.: Handbook of Mathematical Functions With Formulas, Graphs, and Mathematical Tables. Nat. Bur. Stand., Appl. Math. Ser. 55, U.S. Dep. Com., June 1964.

TABLE I.- DATA FOR DUCTED PROPELLER TESTED IN REFERENCE 1

T	6921 N (1556 lbf)
Q	2766 J (2040 ft-lbf)
Ω	2000 rpm = 209 rad/sec
b	1.067 m (3.5 ft)
B	3
γ	0.27 rad
σ	0.2
c	335 m/sec (1100 ft/sec)

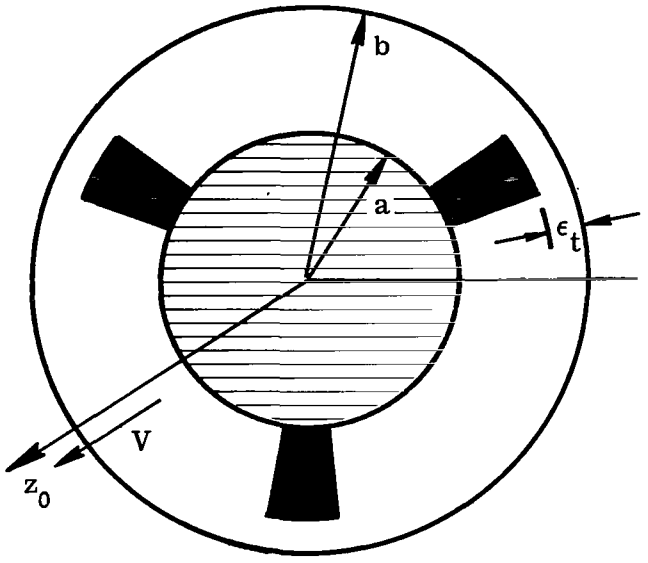

(a) Cross section of disk and duct.

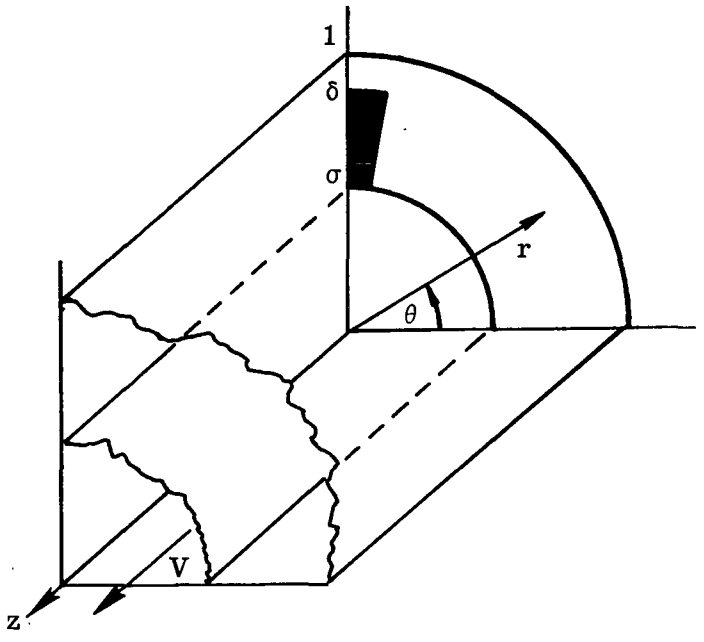

(b) Coordinate system associated with its mathematical model.

Figure 1.- Schematic of ducted-propeller disk.

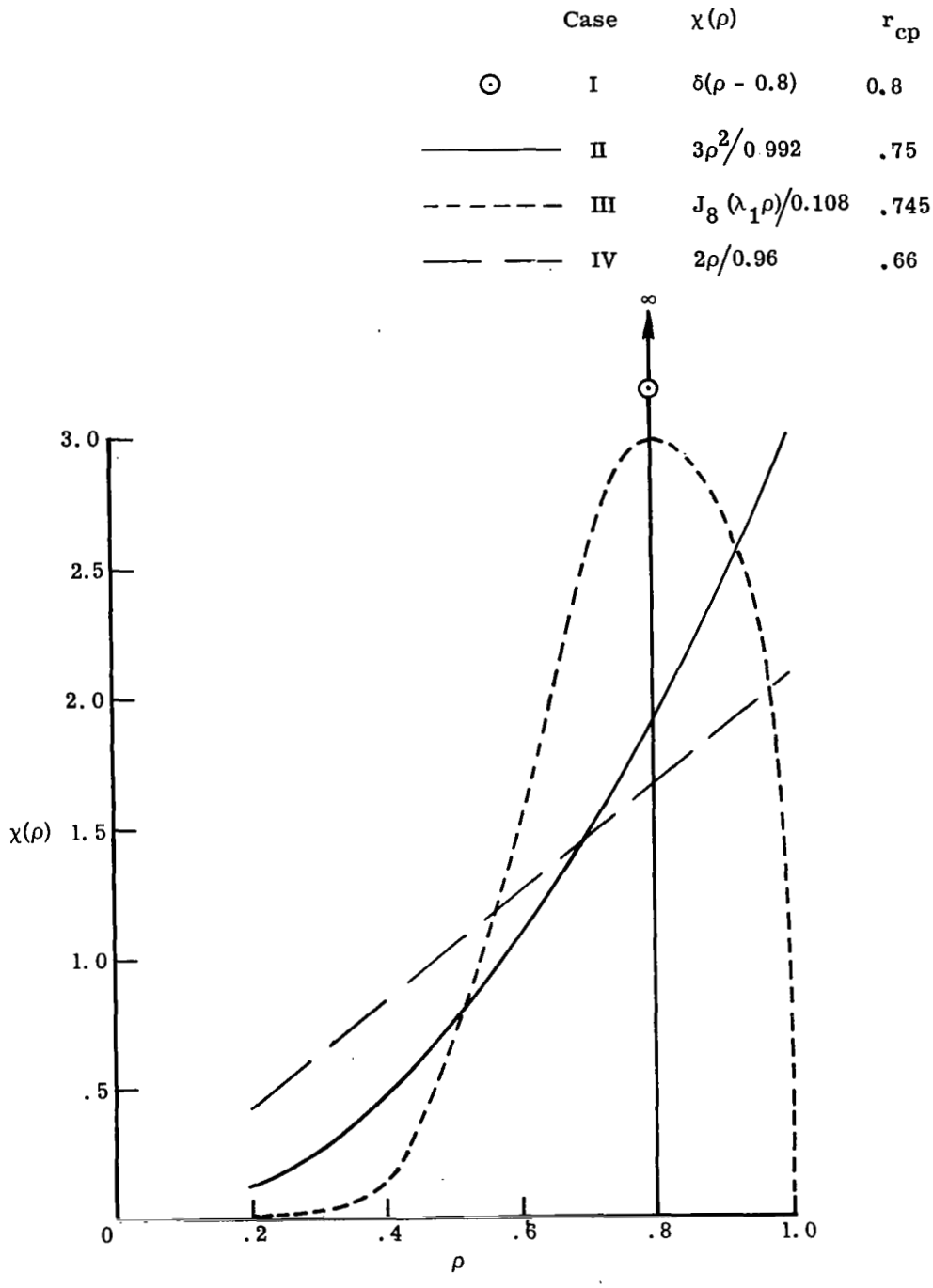

Figure 2.- Four basic propeller loadings $\chi(\rho)$, where $\chi(\rho)$ is representative of either $\frac{B\rho\, T(\rho)}{T}$ or $\frac{B\, Q(\rho)}{\rho Q}$. $\sigma = 0.2$.

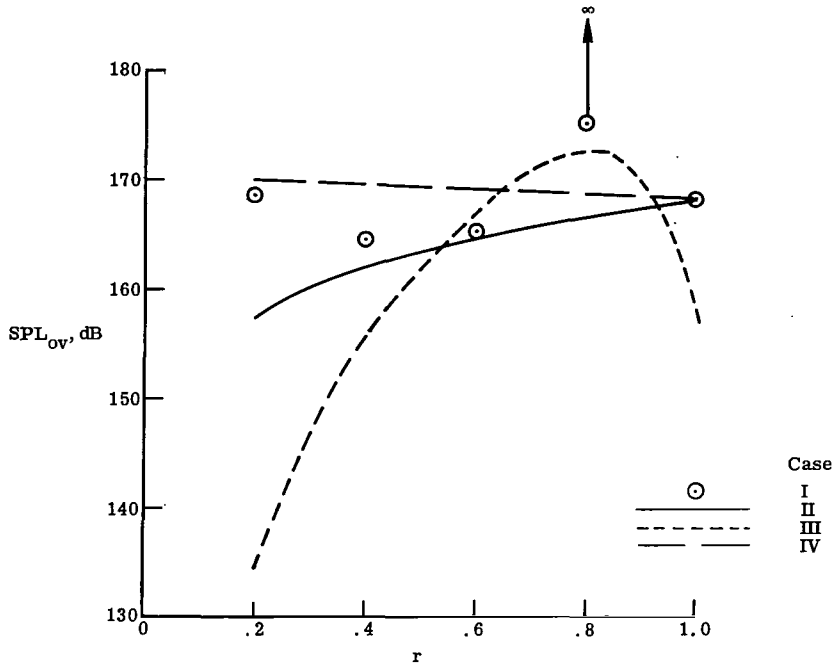

Figure 3.- Radial variation of sound-pressure level at propeller disk at $z = 0$. $M = 0$.

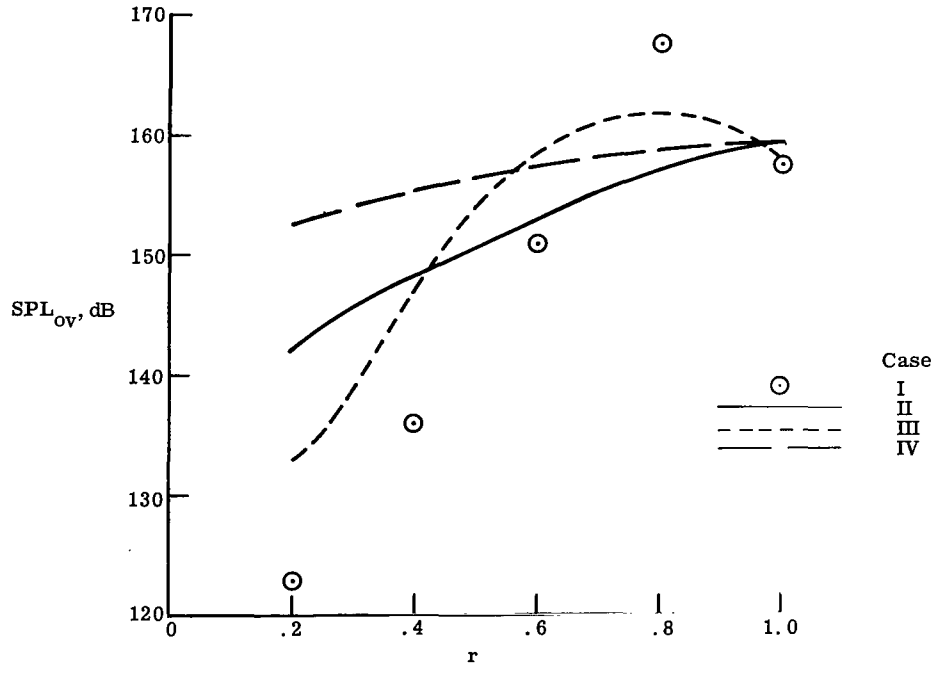

Figure 4.- Radial variation of sound-pressure level at station $z = 0.1$. $M = 0$.

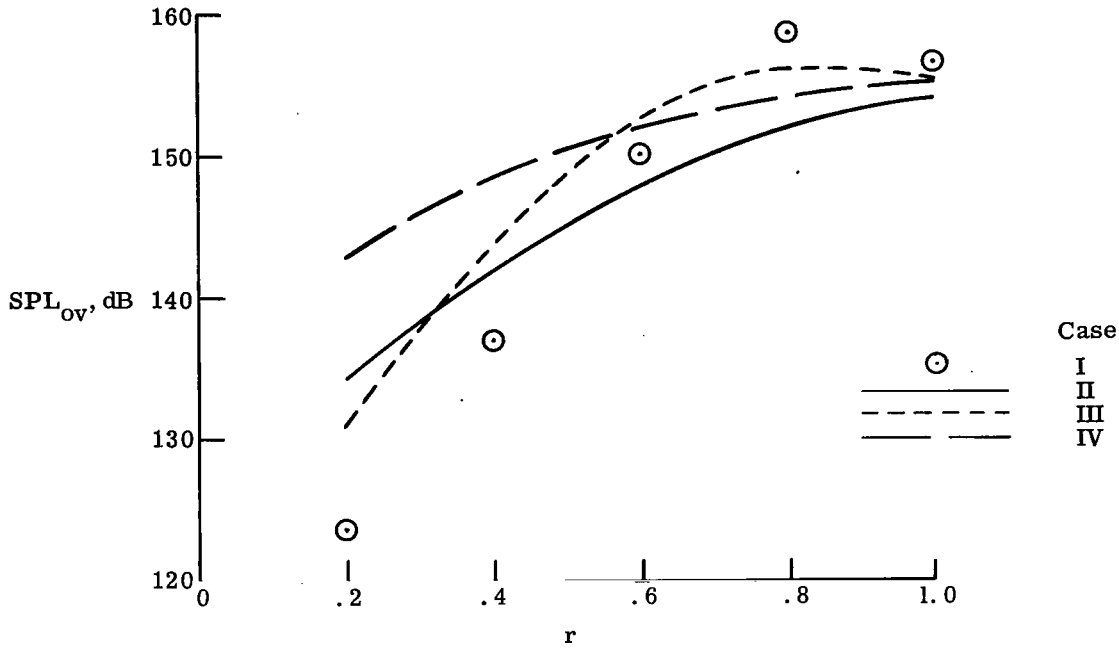

Figure 5.- Radial variation of sound-pressure level at station z = 0.2. M = 0.

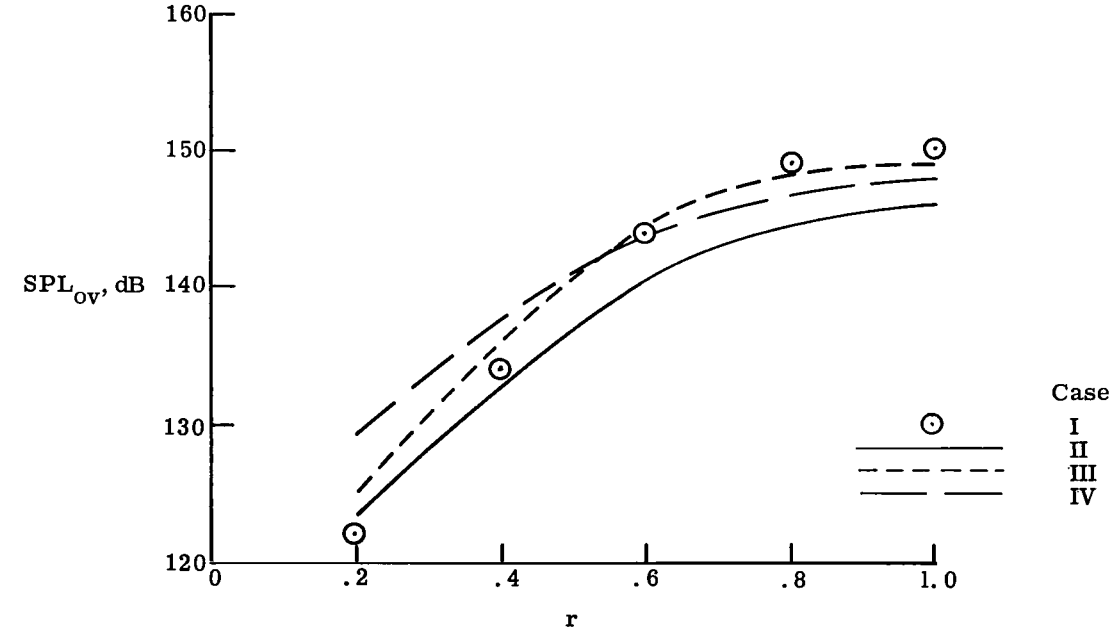

Figure 6.- Radial variation of sound-pressure level at station z = 0.4. M = 0.

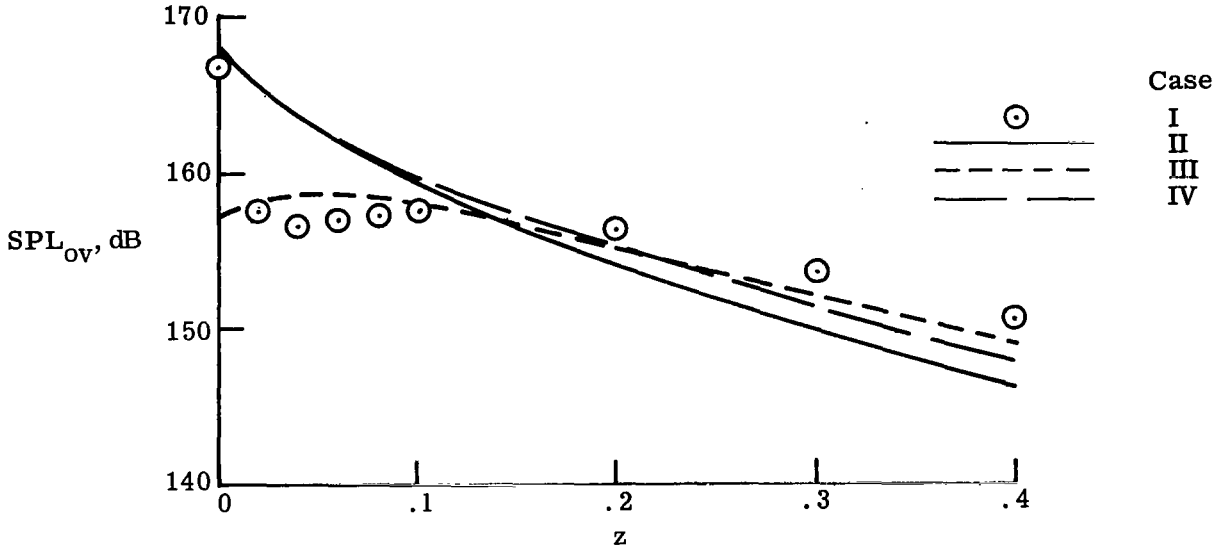

Figure 7.- Variation of sound-pressure level along duct wall at r = 1.0. M = 0.

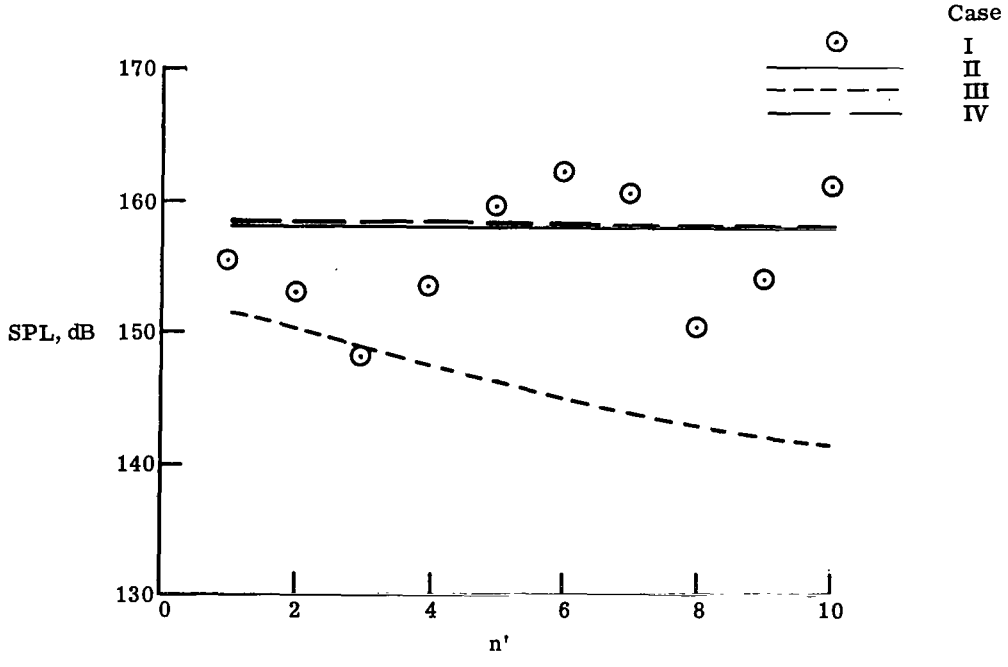

Figure 8.- Variation of sound-pressure level with harmonic number at station z = 0. r = 1.0; M = 0.

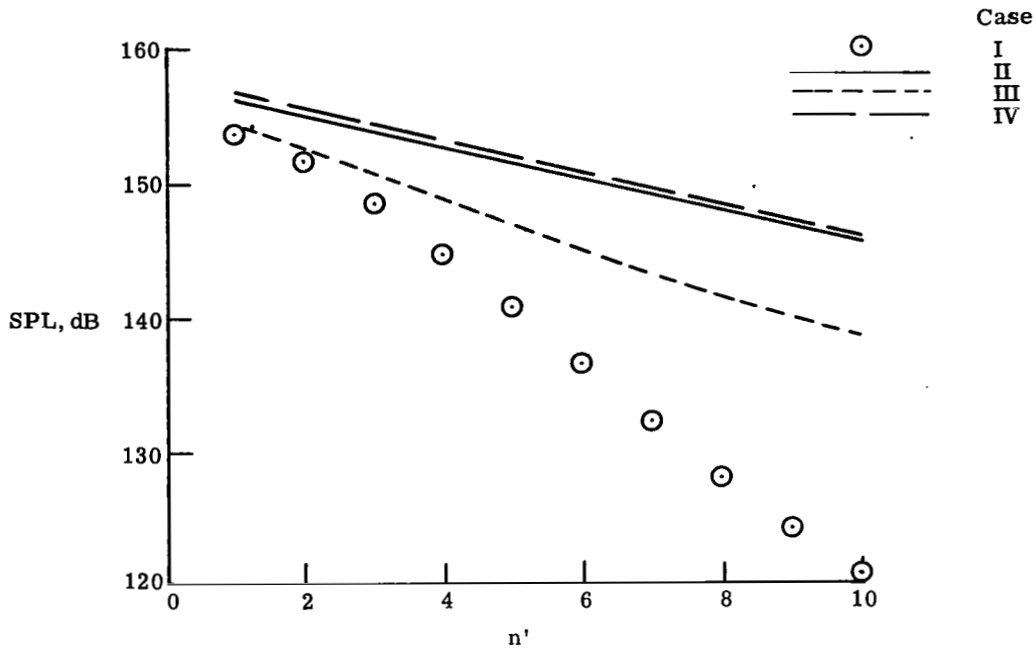

Figure 9.- Variation of sound-pressure level with harmonic number at station z = 0.06. r = 1.0; M = 0.

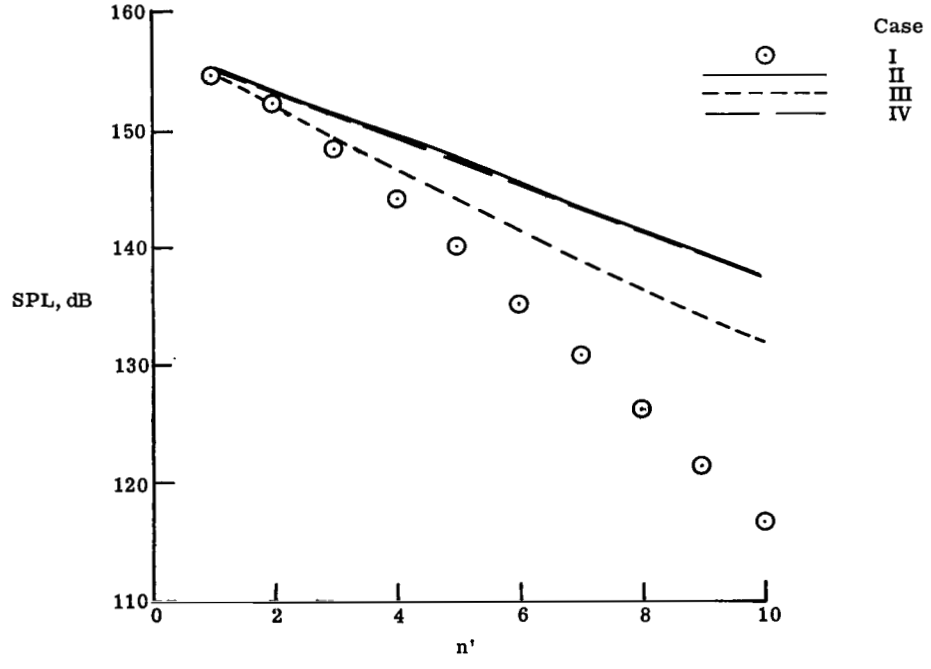

Figure 10.- Variation of sound-pressure level with harmonic number at station z = 0.1. r = 1.0; M = 0.

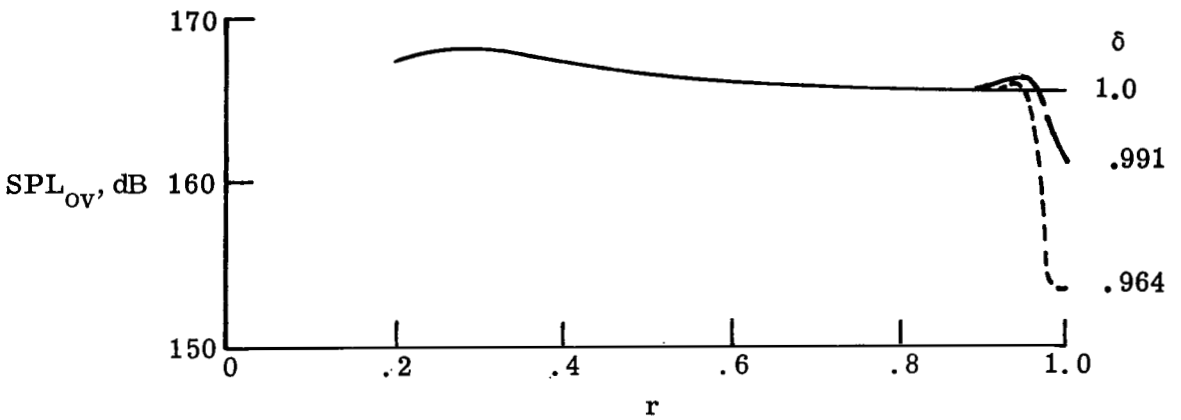

Figure 11.- Effect of tip clearance on sound-pressure level in radial direction at z = 0. M = 0; T = 5224.6 N (1174.6 lbf); Q = 1783 J (1315 ft-lbf); Case IV.

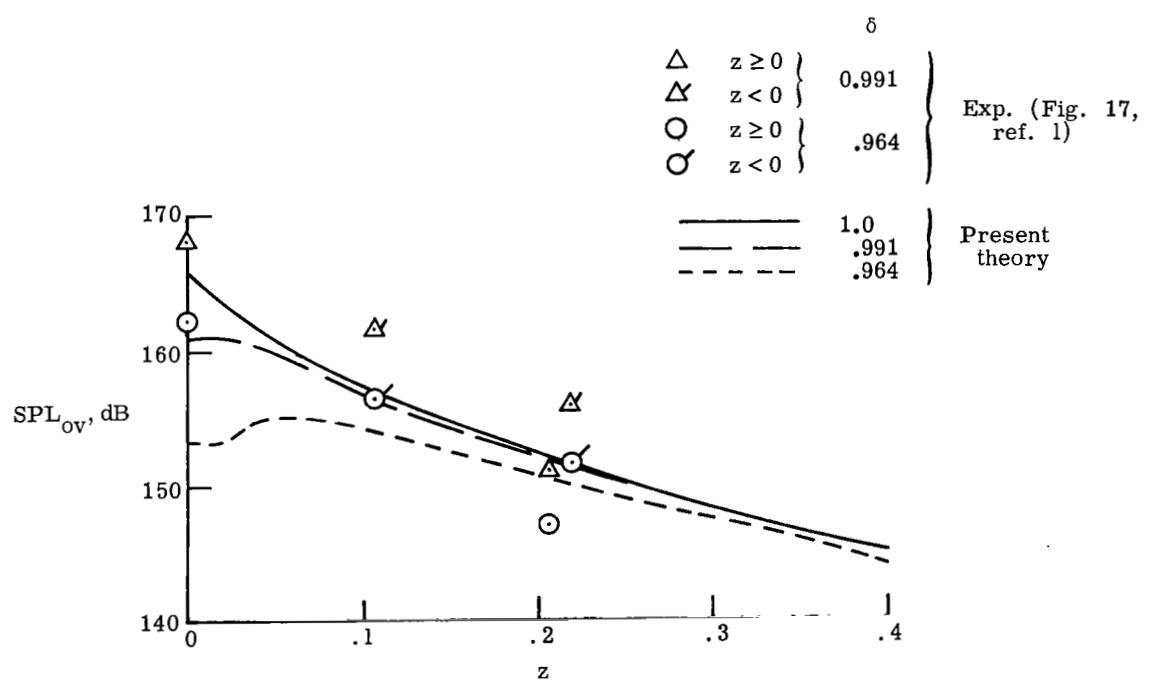

Figure 12.- Effect of tip clearance on sound-pressure level along duct wall at r = 1.0. M = 0; T = 5224.6 N (1174.6 lbf); Q = 1783 J (1315 ft-lbf); Case IV.

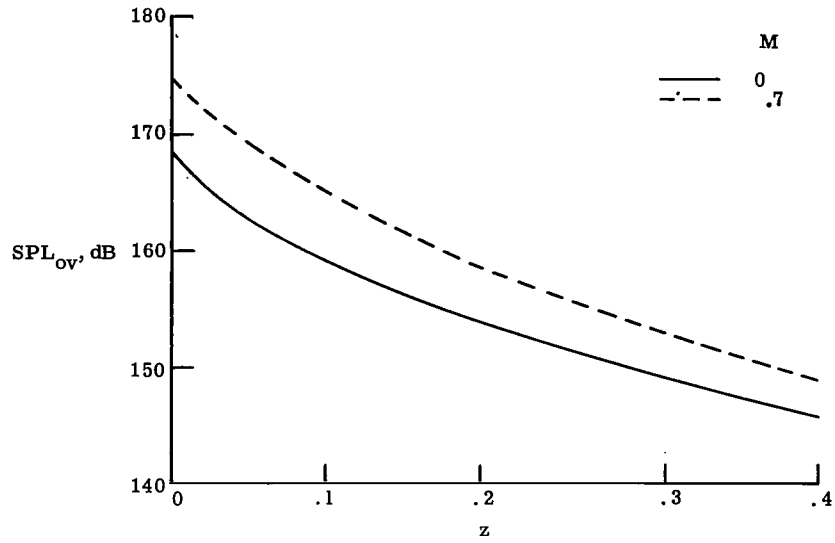

Figure 13.- Effect of free-stream Mach number (M = 0 and M = 0.7) on sound-pressure level in downstream direction for r = 1. Case II.

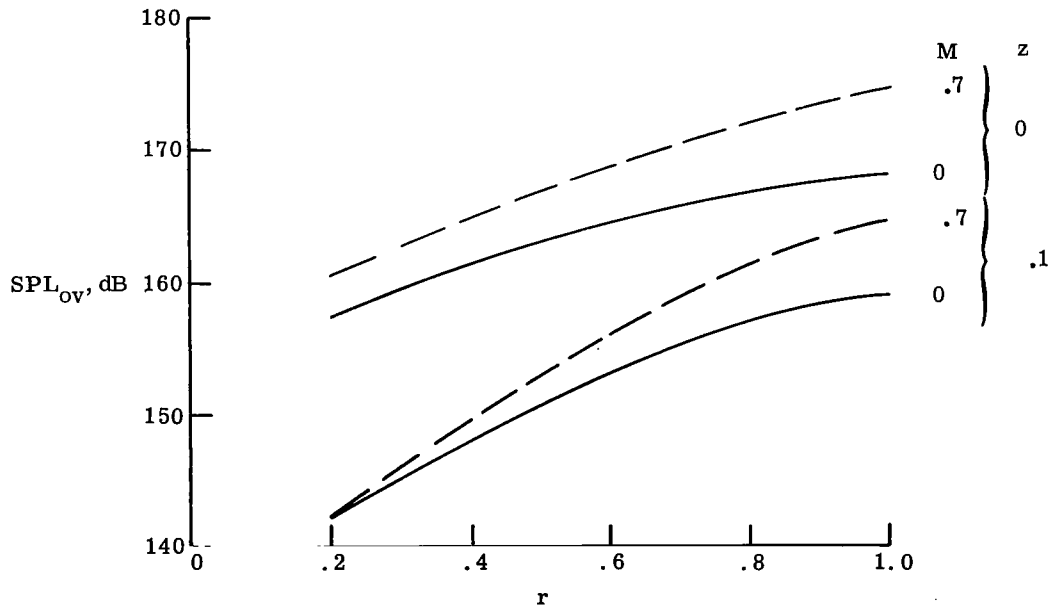

Figure 14.- Effect of free-stream Mach number (M = 0 and M = 0.7) on radial pressure distribution at two downstream locations, z = 0 and z = 0.1. Case II.

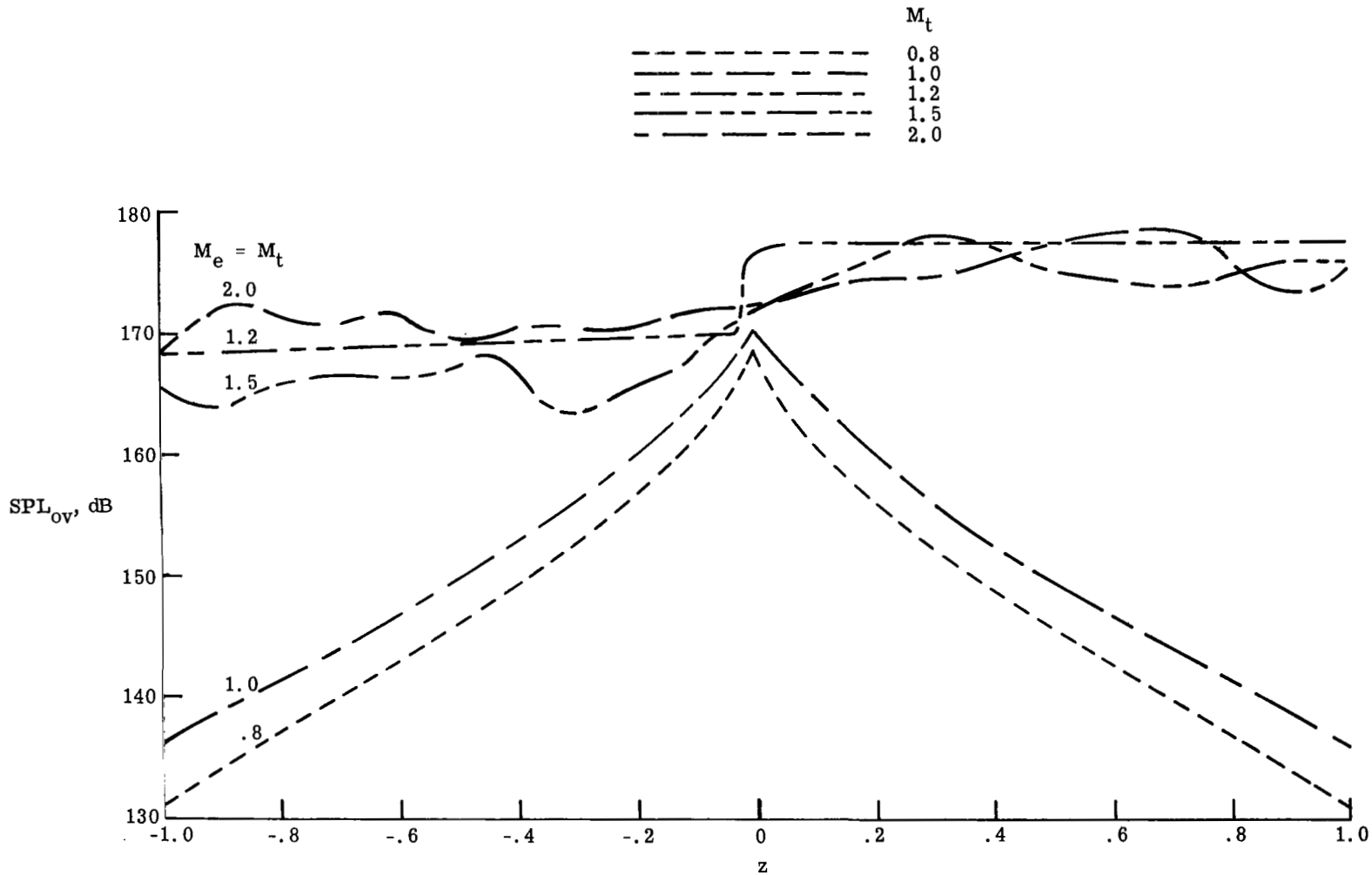

Figure 15.- Effect of rotational tip Mach number on sound-pressure level for $M = 0$. $r = 1.0$; Case IV.

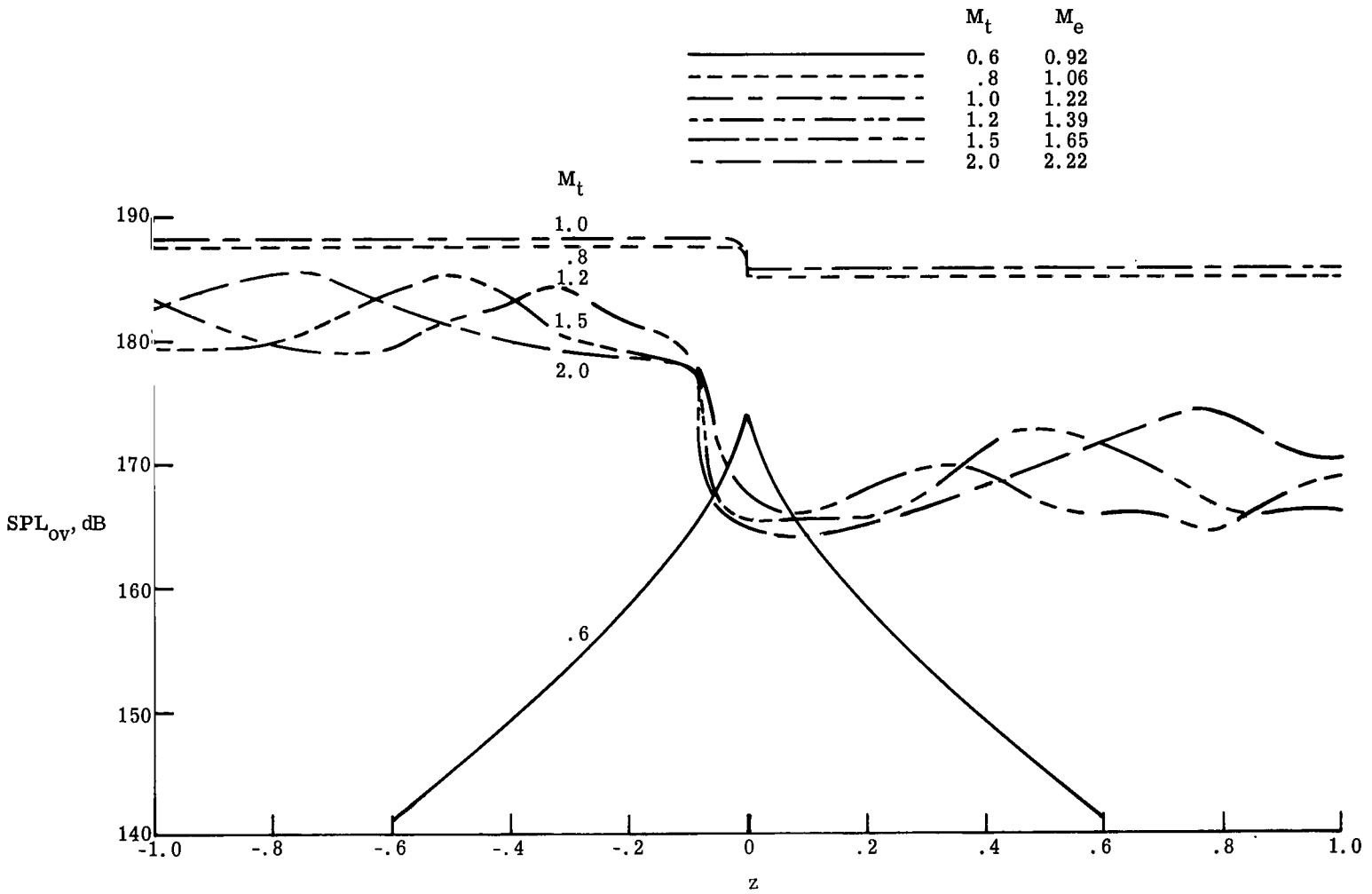

Figure 16.- Effect of rotational tip Mach number on sound-pressure level for M = 0.7. r = 1.0; Case IV.

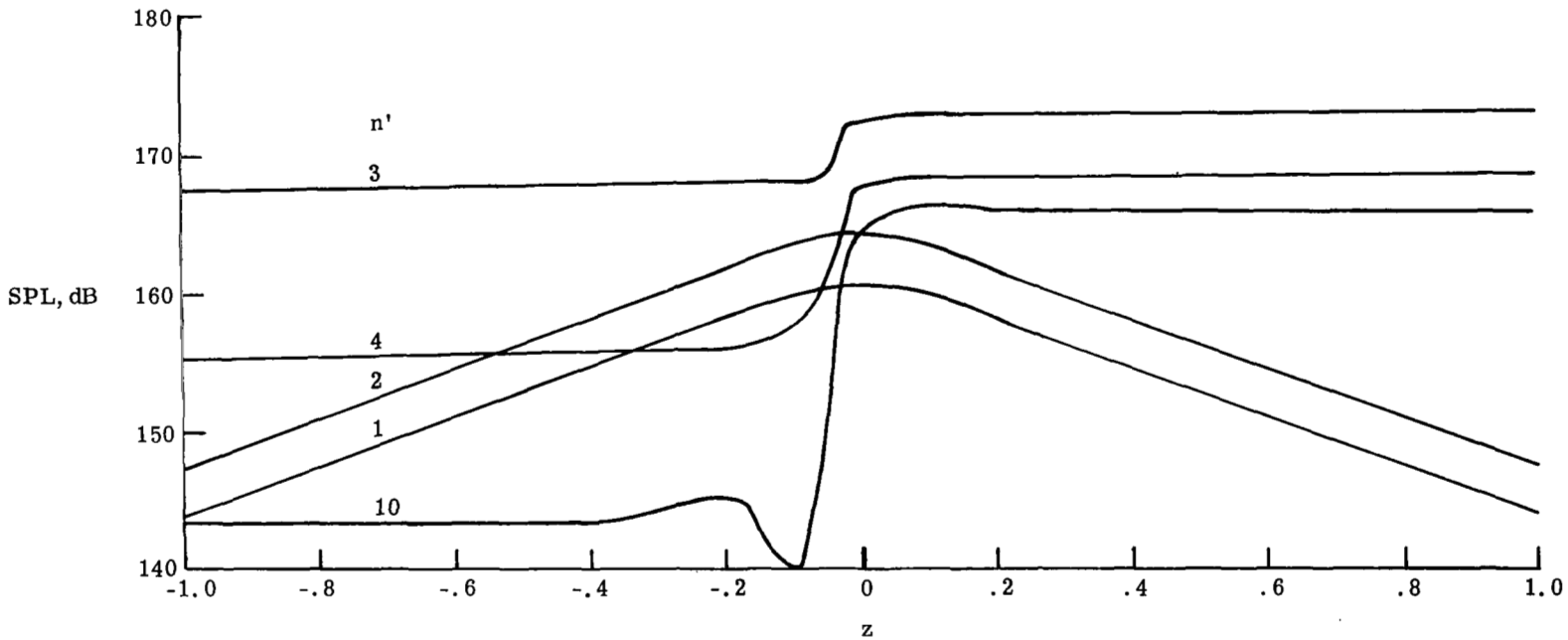

Figure 17.- Harmonic content of duct-wall pressure for $M = 0$ and $M_t = 1.2$. $r = 1$; Case IV.

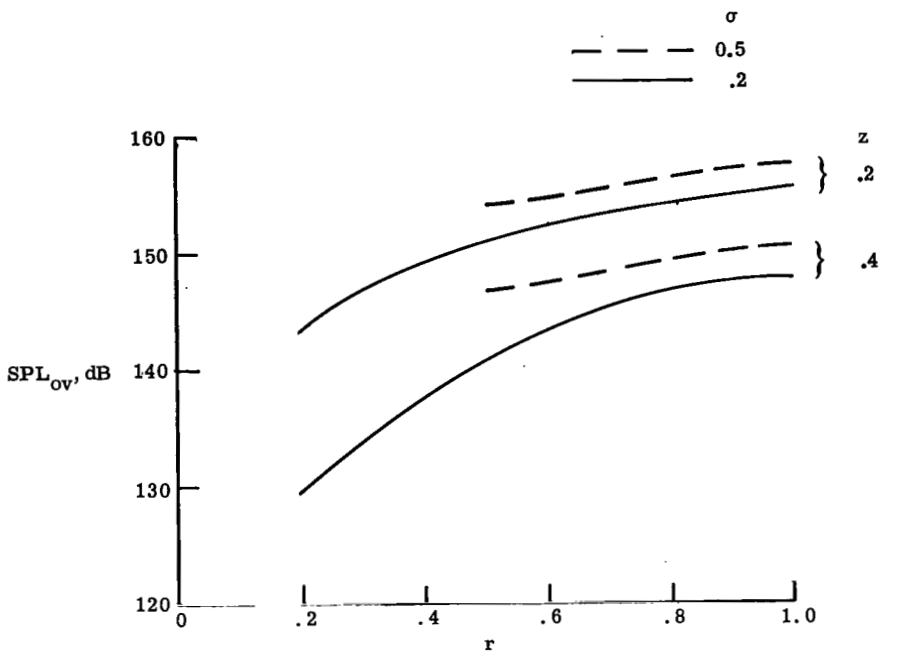

Figure 18.- Radial variation of sound-pressure level for values of hub-tip ratio of $\sigma = 0.2$ and $\sigma = 0.5$ at $z = 0.2$ and $z = 0.4$. $M = 0$; Case IV.

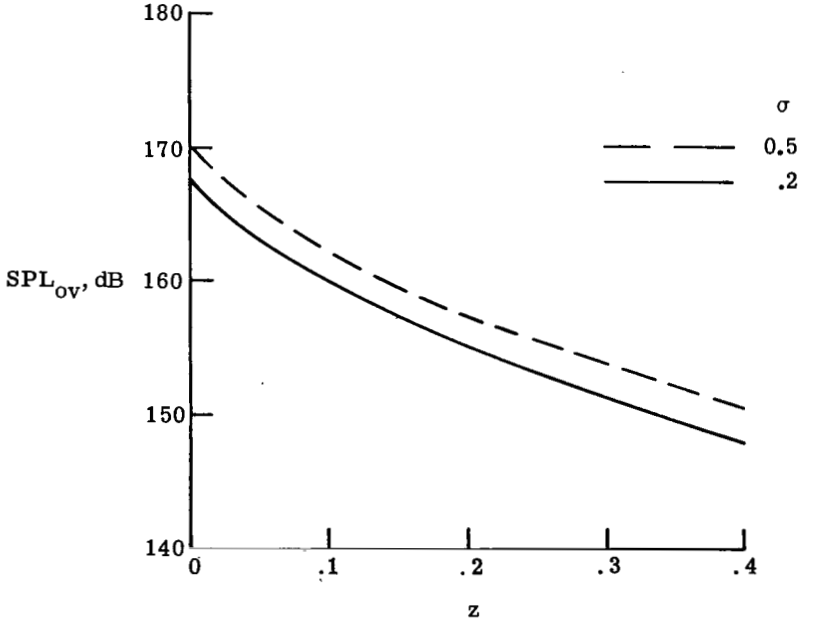

Figure 19.- Variation of sound-pressure level at duct wall for values of hub-tip ratio of $\sigma = 0.2$ and $\sigma = 0.5$. $M = 0$; $r = 1.0$; Case IV.

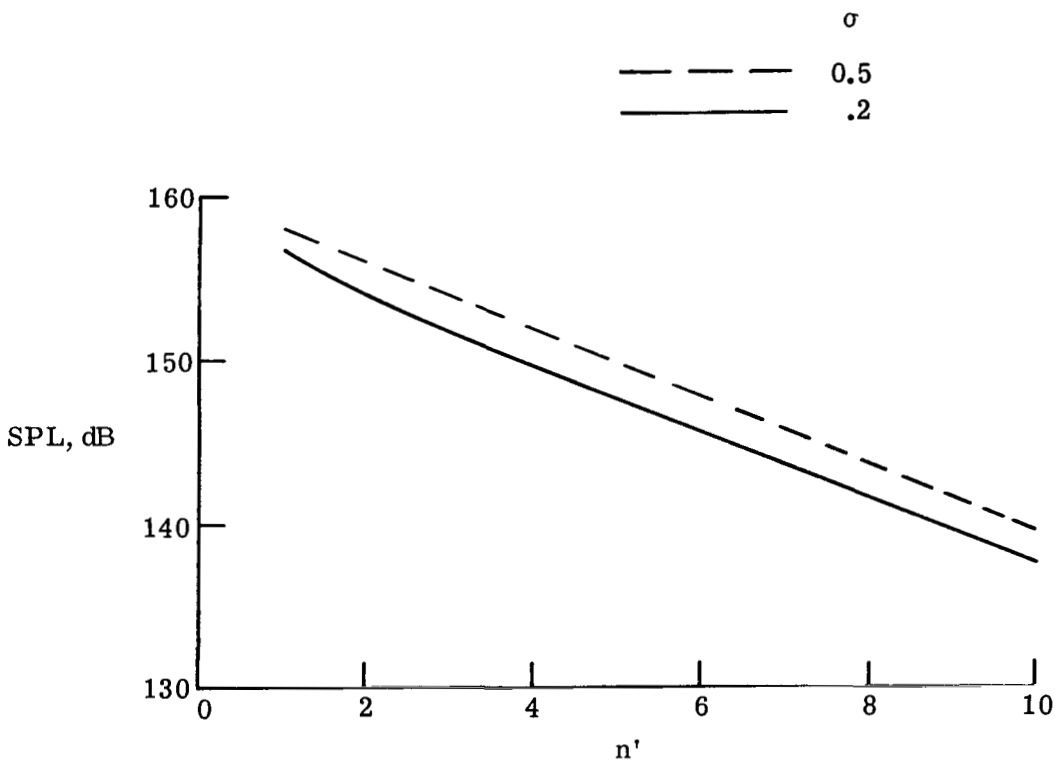

Figure 20.- Variation of sound-pressure level with harmonic number for values of hub-tip ratio of $\sigma = 0.2$ and $\sigma = 0.5$. $z = 0.1$; $M = 0$; $r = 1.0$; Case IV.

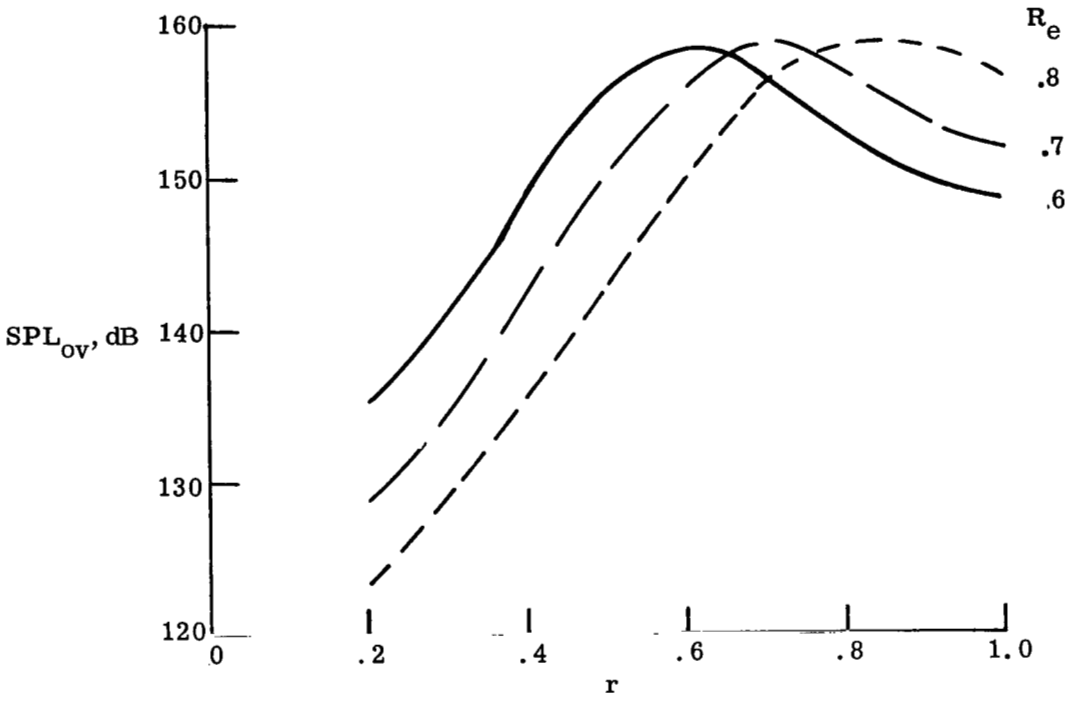

(a) z = 0.2.

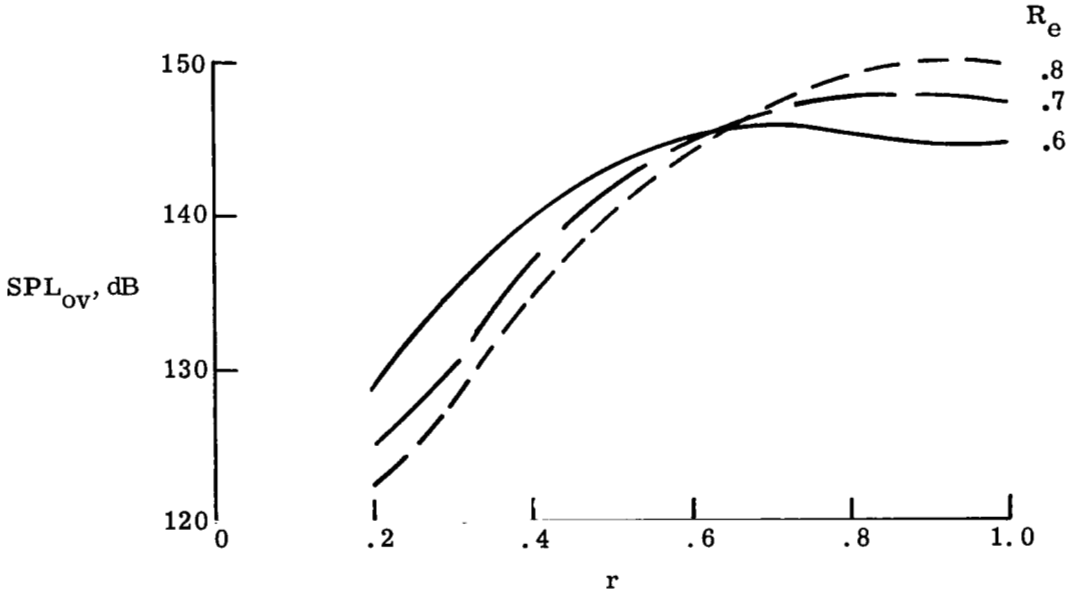

(b) z = 0.4.

Figure 21.- Radial variation of sound-pressure level for values of effective radius $R_e = 0.8$, $R_e = 0.7$, and $R_e = 0.6$ at z = 0.2 and z = 0.4. M = 0; Case I.

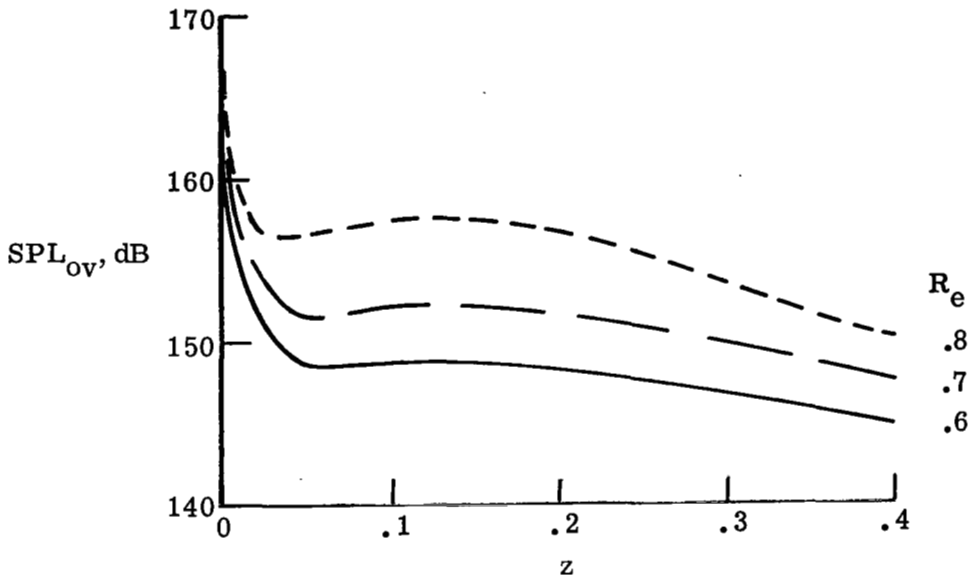

Figure 22.- Variation of sound-pressure level along duct wall for values of effective radius $R_e = 0.8$, $R_e = 0.7$, and $R_e = 0.6$. $M = 0$; $r = 1.0$; Case I.

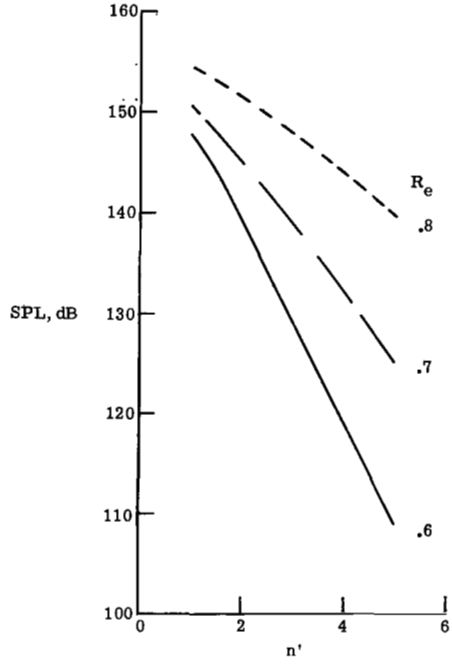

Figure 23.- Variation of sound-pressure level with harmonic number for values of effective radius $R_e = 0.8$, $R_e = 0.7$, and $R_e = 0.6$. $z = 0.1$; $M = 0$; $r = 1.0$; Case I.

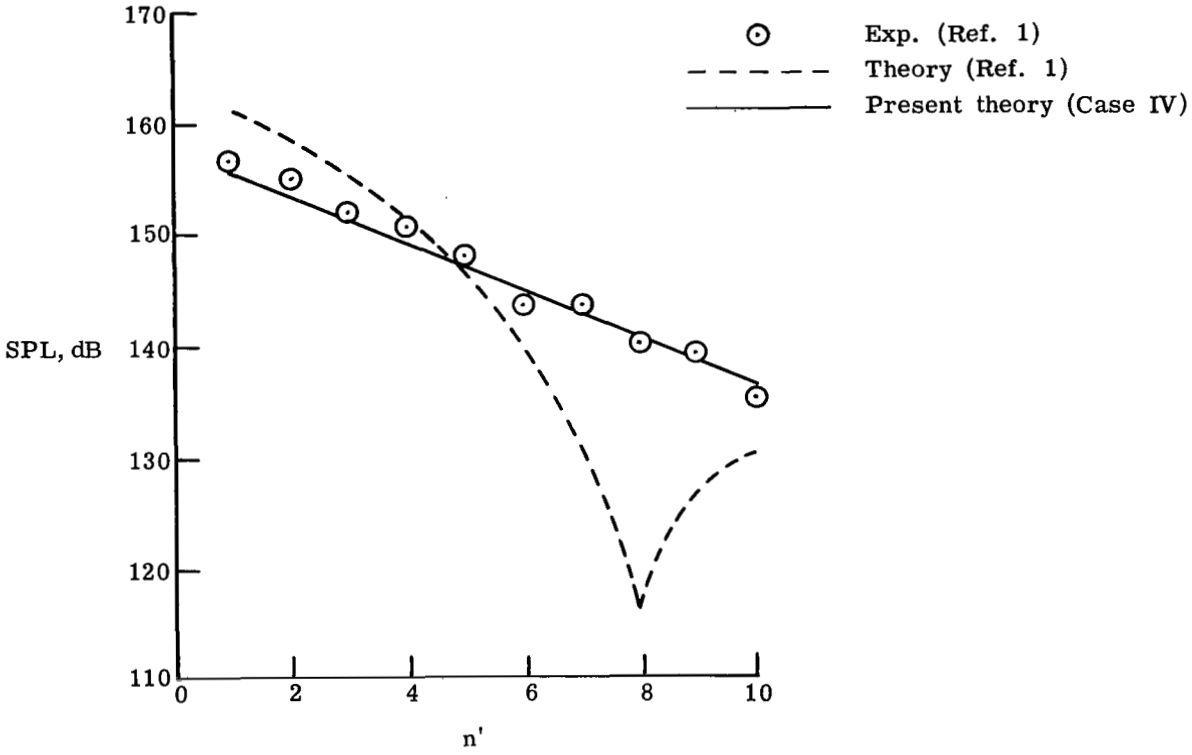

Figure 24.- Comparison of experimental and theoretical results shown in figure 31 of reference 1 with results of present analysis. z = 0.104; M = 0; r = 1.0; Case IV.

NATIONAL AERONAUTICS AND SPACE ADMISTRATION
WASHINGTON, D.C. 20546

OFFICIAL BUSINESS
PENALTY FOR PRIVATE USE $300

FIRST CLASS MAIL

POSTAGE AND FEES PAID
NATIONAL AERONAUTICS AND
SPACE ADMINISTRATION

U.S.MAIL

018 001 C1 U 01 710910 S00903DS
DEPT OF THE AIR FORCE
AF SYSTEMS COMMAND
AF WEAPONS LAB (WLOL)
ATTN: E LOU BOWMAN, CHIEF TECH LIBRARY
KIRTLAND AFB NM 87117

POSTMASTER: If Undeliverable (Section 158 Postal Manual) Do Not Return

"The aeronautical and space activities of the United States shall be conducted so as to contribute . . . to the expansion of human knowledge of phenomena in the atmosphere and space. The Administration shall provide for the widest practicable and appropriate dissemination of information concerning its activities and the results thereof."

— NATIONAL AERONAUTICS AND SPACE ACT OF 1958

NASA SCIENTIFIC AND TECHNICAL PUBLICATIONS

TECHNICAL REPORTS: Scientific and technical information considered important, complete, and a lasting contribution to existing knowledge.

TECHNICAL NOTES: Information less broad in scope but nevertheless of importance as a contribution to existing knowledge.

TECHNICAL MEMORANDUMS: Information receiving limited distribution because of preliminary data, security classification, or other reasons.

CONTRACTOR REPORTS: Scientific and technical information generated under a NASA contract or grant and considered an important contribution to existing knowledge.

TECHNICAL TRANSLATIONS: Information published in a foreign language considered to merit NASA distribution in English.

SPECIAL PUBLICATIONS: Information derived from or of value to NASA activities. Publications include conference proceedings, monographs, data compilations, handbooks, sourcebooks, and special bibliographies.

TECHNOLOGY UTILIZATION PUBLICATIONS: Information on technology used by NASA that may be of particular interest in commercial and other non-aerospace applications. Publications include Tech Briefs, Technology Utilization Reports and Technology Surveys.

Details on the availability of these publications may be obtained from:

SCIENTIFIC AND TECHNICAL INFORMATION OFFICE

NATIONAL AERONAUTICS AND SPACE ADMINISTRATION

Washington, D.C. 20546